# 國 立 交 通 大 學

## 應用化學系分子科學研究所


## 碩 士 論 文

# 硝酸在二氧化鈦表面的吸附及反應情形

# Adsorption Configurations and Reactions of Nitric Acid on $TiO_2$ Rutile (110) and Anatase (101) surface


研 究 生：張靜怡

指導教授：林明璋　院士



中華民國 九十七 年 七 月

# 硝酸在二氧化鈦表面的吸附及反應情形

# Adsorption Configurations and Reactions of Nitric Acid on $TiO_2$ Rutile (110) and Anatase (101) surface


研 究 生：張靜怡　　Student：Ching Yi Chang

指導教授：林明璋 院士　　Advisor：M. C. Lin

國 立 交 通 大 學

應用化學系分子科學研究所


碩 士 論 文

A Thesis

Submitted to Department of Applied Chemistry and Institute of Molecular Science

National Chiao Tung University

in partial Fulfillment of the Requirements

for the Degree of Master

in

Applied Chemistry

July 2008

Hsinchu, Taiwan

中華民國 九十七年七月

# 硝酸在二氧化鈦表面的吸附及反應情形

研 究 生：張靜怡　　指導教授：林明璋 院士

國立交通大學應用化學系分子科學研究所

## 摘　要

本論文藉由 VASP(Vienna Ab-initio Simulation Package) 計算軟體中的理論計算方法，電子密度泛函理論(Density Functional Theory)及超軟贋位勢近似法(Ultrasoft pseudopotential approximation, US-PP)來探討單分子硝酸及雙分子硝酸分別在二氧化鈦金紅石(rutile)(110)表面及銳鈦礦(anatase)(101)表面吸附結構及可能的反應路徑。

從我們的計算結果中可知，單分子硝酸中的氧原子和二氧化鈦金紅石表面上的 $Ti_{5c}$ 形成單一鍵結，而且硝酸分子中的 H 原子與表面的 $O_{2c}$ 形成 H 鍵是最穩定的結構，其吸附能為 6.7 kcal/mol。此硝酸分子的 H 原子可以解離至表面上最鄰近的 $O_{2c}$ 上，此反應步驟幾乎不需要任何的能障就可以生成 $NO_3$(a) + H(a)的結構 。然後，$NO_3$ 分子可以旋轉 $Ti_{5c}$-O 鍵而形成 $Ti_{5c}$-ON(O)-$Ti_{5c}$,H-$O_{2c}$(a)的結構，但需要跨越 12.2 kcal/mol 的能障，$Ti_{5c}$-ON(O)-$Ti_{5c}$,H-$O_{2c}$(a)的吸附能為 16.5 kcal/mol。

在雙分子硝酸吸附的型態中，最穩定的結構是以兩個最穩定單分子的結構組成 2($Ti_{5c}$–ON(O)OH…$O_{2c}$(a))，其吸附能為 12.8 kcal/mol。從 2($Ti_{5c}$–ON(O)OH…$O_{2c}$(a)) 形成 $N_2O_5$ 分子需要跨越 46.2 kcal/mol 的能障，由此可知聚合反應難以發生。單分子及雙分子硝酸在二氧化鈦銳鈦礦表面的吸附及反應路徑和在金紅石表面相似。

另外， 由上述反應中，我們發現 H 原子吸附在 $O_{2c}$ 上在吸附能上扮

演一個重要的角色，特別是對 $NO_3$ 自由基。$NO_3$ 可能成為一個有效的連接分子以連接半導體量子點系統，例如：氮化銦(InN)半導體量子點，和二氧化鈦表面。此外，我們也進一步計算以 $NO_3$ 連接氮化銦團簇$(InN)_X$ 及二氧化鈦表面的電子分佈狀況。

# Adsorption Configurations and Reactions of Nitric Acid on $TiO_2$ Rutile (110) and Anatase (101) surfaces

Student：Ching Yi Chang　　Advisor：M. C. Lin

Institute of Molecular Science
National Chiao Tung University

## Abstract

The adsorption and reactions of the monomer and dimer of nitric acid on $TiO_2$ rutile (110) and anatase (101) surfaces have been studied by first-principles calculations based on the density functional theory in conjunction with ultrasoft pseudopotential approximation implemented in the Vienna Ab-initio Simulation Package (VASP).

The most stable configuration of $HNO_3$ on the rutile surface is a molecular monodentate adsorbed on the 5-fold coordinated Ti atom with the hydrogen bonded to a neighboring surface bridging oxygen with the adsorption energy of 6.7 kcal/mol. It can dissociate its H atom to a nearest bridged oxygen with approximately no barrier to produce $NO_3$(a) + H(a). The rotation of $NO_3$ requires a barrier of 12.2 kcal/mol to form the by didentate configuration $Ti_{5c}$-ON(O)-$Ti_{5c}$,H-$O_{2c}$(a), which adsorbs on two 5-fold coordinated Ti atoms with the adsorption energy of 16.5 kcal/mol.

In the case of the adsorption of $2HNO_3$ molecules, the most stable configuration, 2($Ti_{5c}$–ON(O)OH…$O_{2c}$(a)), has a structure similar to two single $HNO_3$ adsorbates on two 5-fold coordinated Ti atoms with the adsorption

energy of 12.8 kcal/mol, which is about twice that of the single $HNO_3$ molecule. The result suggests that the interaction of the two planar $HNO_3$ adsorbates is negligible. The dehydration from $2(Ti_{5c}\text{–}ON(O)OH\ldots O_{2c}(a))$ forming $N_2O_5$ requires an energy barrier of 46.2 kcal/mol, indicating that the dimerization of the two $HNO_3(a)$ is hard to occur. Similar adsorption phenomena appear on the anatase (101) surface.

The result of our calculations shows that the co-adsorption of hydrogen plays a significant role in the adsorption energies of adsorbates, especially for the $NO_3$ radical, which may be employed as a linker between semiconductor quantum dots such as InN with the $TiO_2$ surface. Furthermore, we calculate the charge distribution of the $NO_3$ group connecting (InN)x clusters with $TiO_2$.

# Acknowledgements

這兩年對我而言是很特別的一段日子，沒有念大學的主科—物理，反而念了一樣是基礎科學的化學，有時候有點迷惘，有時候又覺得選一條有挑戰的路也是挺有意思的。

在這些日子裡，很感謝我的指導老師—林明璋院士，與老師的談話中，總可以讓我得到一些課本上學不到的東西，帶我看到不一樣的世界；學問方面也謝謝老師的教導，總能有不同的見解。從老師身上看到的態度是遠遠比這兩年中學到的知識要重要得多，這些態度對我有一定程度的影響！“Where there is a will, there is a way”對嗎?

其次感謝的就是朱超原、王念夏教授和林聖賢院士，在碩一上當朱超原老師的助教時，了解原來做學問要抱持著很嚴謹的態度，如何扎扎實實的做學問，以及老師在碩一下計算化學課程的教導，讓我從門外漢探進門內，看到這屬於學問的美。感謝王念夏老師，總能給我一些協助，並且可以把問題都簡單化，讓我了解原來可以以輕鬆的態度面對困難。也謝謝林聖賢院士能在碩士班口試時當我的口試委員，謝謝院士當天的笑容與鼓勵，口試那一天對我而言是難忘的!

在碩士論文中，也感謝陳欣聰博士的指導，對於我這個愛問問題的學生，總是能給予一定程度的解答。也謝謝秀琴，禎翰學長，雯妃學姐，老王學長，佩儀學妹，實驗室的大家及在交大的老伴琇雅和春慧。

這篇致謝也同時與疼我的外婆、放心不下我的老媽、超信任我的老爸、適時關心我的老哥分享與遠在台南的廷璁男友分享。台北的家和中壢的外婆家始終是我的避風港，謝謝你們無怨無悔的包容與支持!

謝謝大家!

# Table of Contents

page

# List of Figures

# List of Tables

# Chapter One

# Introduction

## 1-1 Preface

In the 21th century, we face the crisis in energy resources. We will run out of petroleum within forty years. We are also facing the detrimental effect of greenhouse gases, $CO_2$ in particular, produced from fossil fuel combustion. It is vital for us to search for environmentally clean alternative energy resources. A renewable energy such as solar radiation is ideal to meet the projected demand but requires new strategies to harvest incident photons with a higher efficiency, for example, by employing nano-structured semiconductors and molecular assemblies.

## 1-2 Discussion on $TiO_2$ research field

In 1991, Grätzel et al.[1] invented the dye-sensitized solar cells (DSSC) system using $TiO_2$ nano particle films. Organic dye molecules were attached on the porous $TiO_2$ structures as absorbate which provided an alternative photovoltaic device for electricity generation. The overall energy conversion (light to electricity) was typically 7.1%~7.9% in 1991. In DSSC system[2], charges on the $TiO_2$ interface go from photo-excited dye to the conduction band of the semiconductor. The sunlight in the range between the wavelengths from the UV to the near IR region has a broad spectral adsorption for energy conversion. The efficiency may reach over 10%. However, dyes (N3 dye) are relatively expensive, and organic compounds have shorter lifetimes and are less stable than inorganic materials. Many researchers, therefore, prefer to employ semiconductor quantum dots (QD) instead of dyes for solar cells.

Moreover, $TiO_2$ has been studied broadly for its physical and chemical characteristic and applications , such as in heterogeneous photocatalysis on surfaces[3,4], the nature of photovoltaic action[5,6] and nanomaterial[7] properties. All the previous information provides a rich scientific basis on its potential solar cell development.

Furthermore, investigating all the rich properties of titanium dioxide not only depend on experiments, but also on theoretical studies. Experiments and theoretical calculations are complementary to each other. We can know the reaction mechanisms in detail by theoretical calculations. The advantage of theoretical calculations is that it can reveal the mechanism of a reaction which we can not obtain through experiment and these save more expensive cost in experiment. Theoretical results contain rich and many-sided views on various effects such as doping (N-doped[8,9], C-doped[10] and S-doped[11]) and vacancy(O-vac[12]) of titanium dioxide surfaces. Recently more and more studies on semiconductor quantum dots[13] (GaN[14], InN[15-17], AlN[18], InP[19]) have been made by theoretical calculations. Further studies of quantum-dot sensitized $TiO_2$ solar cells (QDSSC), by which their optical properties can maximize solar photon adsorption, have been carried out, for example, Wang et al.[20] reported that the absorption spectrum of InN/$TiO_2$ films showed a pronounced broad band absorption in the UV-Vis range, covering 390-800 nm, similar to Grätzel's black dye. $TiO_2$ solar cell with InAs[21] quantum dots has also been studied. In these systems, in order to achieve higher efficiencies, it is essential to find a good linker between quantum dots (InN, InAs…) and the $TiO_2$ surface.

In our lab, we have studied the $HN_3$/TMIn[22,23] reaction to produce InN quantum dots on $TiO_2$ fabricated films and have analyzed adsorption/reaction of $H_3BO_3$[24], $H_2S$[25] and $H_2O_2$[26] experimentally and theoretically. In the present

work, we want to investigate the adsorption and reaction of nitric acid ($HNO_3$) on $TiO_2$ surfaces and compare the chemistry with the Boric acid ($H_3BO_3$)/$TiO_2$ system[24]. We regard $HNO_3$ as a potential linker group[27] to connect InN clusters with $TiO_2$.

## 1-3 Reference


(1) O'Regan, B.; Grätzel, M. *Nature* **1991**, *353*, 737.

(2) Grätzel, M. *Journal of Photochemistry & Photobiology, C: Photochemistry Reviews* **2003**, *4*, 145.

(3) Linsebigler, A. L.; Lu, G.; Yates Jr, J. T. *Chemical Reviews* **1995**, *95*, 735.

(4) Mills, A.; LeHunte, S. *Journal of Photochemistry and Photobiology a-Chemistry* **1997**, *108*, 1.

(5) Cahen, D.; Hodes, G.; Grazel, M.; Guillemoles, J. F.; Riess, I. *J. Phys. Chem. B* **2000**, *104*, 2053.

(6) Durrant, J. R.; Haque, S. A.; Palomares, E. *Chemical Communications* **2006**, *2006*, 3279.

(7) Chen, X.; Mao, S. S. *Chem Rev* **2007**, *107*, 2891.

(8) Asahi, R.; Morikawa, T.; Ohwaki, T.; Aoki, K.; Taga, Y. *Science* **2001**, *293*, 269.

(9) Di Valentin, C.; Pacchioni, G.; Selloni, A. *Physical Review B* **2004**, *70*, 85116.

(10) Di Valentin, C.; Pacchioni, G.; Selloni, A. *Chem. Mater* **2005**, *17*, 6656.

(11) Tian, F.; Liu, C. *J. Phys. Chem. B* **2006**, *110*, 17866.

(12) Mutombo, P.; Kiss, A. M.; Berk, A.; Cháb, V. *Modelling Simul. Mater. Sci. Eng* **2008**, *16*, 025007.

(13) Loss, D.; DiVincenzo, D. P. *Physical Review A* **1998**, *57*, 120.

(14) Yeo, Y. C.; Chong, T. C.; Li, M. F. *Journal of Applied Physics* **1998**, *83*, 1429.

(15) Persson, C.; Ferreira da Silva, A. *Journal of Physics: Condensed Matter* **2001**, *13*, 8945.

(16) Ahmed, R.; Akbarzadeh, H. *Physica B: Physics of Condensed Matter* **2005**, *370*, 52.

(17) Bagayoko, D.; Franklin, L. *Journal of Applied Physics* **2005**, *97*, 123708.

(18) Kandalam, A. K.; Pandey, R.; Blanco, M. A.; Costales, A.; Recio, J. M.; Newsam, J. M. *J. Phys. Chem. B* **2000**, *104*, 4361.

(19) Blackburn, J.; Ellingson, R.; Micic, O.; Nozik, A. *J. Phys. Chem. B* **2003**, *107*, 102.

(20) Wang, J. H.; Lin, M. C. *ChemPhysChem* **2004**, *5*, 1615.

(21) Yu, P.; Zhu, K.; Norman, A. G.; Ferrere, S.; Frank, A. J.; Nozik, A. J. *J. Phys. Chem. B* **2006**, *110*, 25451.

(22) Wang, J. H.; Lin, M. C. *Journal of Physical Chemistry B* **2006**, *110*, 2263.

(23) Tzeng, Y. R.; Raghunath, P.; Chen, S. C.; Lin, M. C. *Journal of Physical Chemistry A* **2007**, *111*, 6781.

(24) Raghunath, P.; Lin, M. C. *J. Phys. Chem. C* **2008**, *112*, 8276.

(25) Huang, W. F.; Chen, H. T.; Lin, M. C. *Chem Phys Lett* **2008**, communicated.

(26) Huang, W. F.; Raghunath, P.; Lin, M. C. *J. Comput. Chem* **2008**, communicated.

(27) Lee, H. J.; Kim, D. Y.; Yoo, J. S.; Bang, J.; Kim, S.; Park, S. M. *Bulletin of the Korean Chemical Society* **2007**, *28*, 953.

# Chapter Two

# Computational methods

## 2-1 Introduction：

VASP (Vienna ab-initio Simulation Package)[1] computational program is based on Density Functional Theory (DFT) which can be used to calculate the electronic ground state of a chemical system including gases and solids.

In this thesis, all the geometrical structures are calculated by VASP on the basis of first-principles[2] with the electron-correlation methods such as LDA (local density approximation and GGA[3] (generalized gradient approximation) at 0K. According to the VASP guide, the interaction between ions and electrons is described by ultra-soft Vanderbilt pseudopotentials (US-PP) or by the projector-augmented wave (PAW) method with a plane basis set. We select US-PP as pseudopotentials in the following calculations, except the Bader Charge which is done with the PAW method.

The following is the introduction of the DFT, Kohn-Sham Theory and NEB methods.

## 2-2 Density Functional Theory (DFT)[4]：

From a single particle Schrödinger equation eq.(1), $\psi(\vec{r})$ is a particle wave function , $\psi^*(\vec{r})$ is a particle conjugate wave function. $\hbar$ is called Dirac constant, which is Plank constant divided by $2\pi$. E is the total energy of the particle including kinetic energy and potential energy. V(r) is the potential energy of the particle. T is the kinetic energy of the particle.

$$H\psi(\vec{r}) = E\psi(\vec{r}) \quad \text{..... (1)}$$

$$E = T + V \quad \text{..... (2)}$$

$$-\frac{\hbar^2}{2m}\nabla^2\psi(\vec{r})+V(r)\psi(\vec{r})=E\psi(\vec{r}) \quad \text{..... (3)}$$

$$-\frac{\hbar^2}{2m}\nabla^2\psi^*(\vec{r})+V(r)\psi^*(\vec{r})=E\psi^*(\vec{r}) \quad \text{..... (4)}$$

Density defined as the probability of wave function

$$\rho(\vec{r})=\psi^*(\vec{r})\psi(\vec{r})=\left|\psi(\vec{r})\right|^2 \quad \text{..... (5)}$$

With Laplacian operator $\nabla^2$ on eq.(5)

$$\nabla^2[\psi^*(\vec{r})\psi(\vec{r})]=\nabla^2[\psi^*(\vec{r})]\psi(\vec{r})+\psi^*(\vec{r})[\nabla^2\psi(\vec{r})]+2\nabla\psi^*(\vec{r})\cdot\nabla\psi(\vec{r})$$

$$=-2\frac{2m}{\hbar^2}[E-V(r)]\rho(\vec{r})+2\nabla\psi^*(\vec{r})\cdot\nabla\psi(\vec{r}) \quad \text{..... (6)}$$

$$(6)\times-\frac{\hbar^2}{4m}$$

$$-\frac{\hbar^2}{4m}\nabla^2\rho(\vec{r})+V(r)\rho(\vec{r})=E\rho(\vec{r})-\frac{\hbar^2}{2m}\nabla\psi^*(\vec{r})\cdot\nabla\psi(\vec{r}) \quad \text{..... (7)}$$

Another polar coordinate expression for $\psi(\vec{r})$ and $\psi^*(\vec{r})$ in eq.(8) and eq.(9)

$$\psi(\vec{r})=\sqrt{\rho(\vec{r})}e^{i\theta(\vec{r})} \quad \text{..... (8)}$$

$$\psi^*(\vec{r})=\sqrt{\rho(\vec{r})}e^{-i\theta(\vec{r})} \quad \text{..... (9)}$$

Combine eq.(8), eq.(9) into eq.(7)

$$\nabla\psi^*(\vec{r})\cdot\nabla\psi(\vec{r})=[\nabla\sqrt{\rho(\vec{r})}]^2+\rho(\vec{r})[\nabla\theta(\vec{r})]^2\approx\frac{1}{4\rho}[\nabla\rho]^2 \quad \text{..... (10)}$$

$$-\frac{\hbar^2}{4m}\nabla^2\rho(\vec{r})+V(r)\rho(\vec{r})\approx E\rho(\vec{r})-\frac{\hbar^2}{8m\rho(\vec{r})}[\nabla\rho(\vec{r})]^2 \quad \text{..... (11)}$$

If we can do $\theta(\vec{r})=\sum_n\lambda^n f_n(\rho)$, we have exact equation equal to solving density equation as solving wave function.

## 2-3 Reduced Density Matrix methods：

The exact solution for wave function of N-electron system, each electron ($\vec{r}_i$) contains 4 variables, three spatial and one spin coordinate.

A wave function $\psi(\vec{r}_1,\vec{r}_2,\vec{r}_3.....,\vec{r}_N)$ for N electron systems contains 4N variables.

In reduced density matrix methods, is ignored electron spin.

$$H_e\psi(\vec{r}_1,\vec{r}_2,\vec{r}_3.....,\vec{r}_N)=E\psi(\vec{r}_1,\vec{r}_2,\vec{r}_3.....,\vec{r}_N) \quad \text{..... (12)}$$

Define the first-order density matrix

$$\gamma_1(\vec{r}_1,\vec{r}_1')=N\int\psi^*(\vec{r}_1',\vec{r}_2,\vec{r}_3.....,\vec{r}_N)\psi(\vec{r}_1,\vec{r}_2,\vec{r}_3.....,\vec{r}_N)d\vec{r}_2d\vec{r}_3.....d\vec{r}_N \quad \text{..... (13)}$$

Define the second-order density matrix

$$\gamma_2(\vec{r}_1,\vec{r}_2,\vec{r}_1',\vec{r}_2')=N(N-1)\int\psi^*(\vec{r}_1',\vec{r}_2',\vec{r}_3.....,\vec{r}_N)\psi(\vec{r}_1,\vec{r}_2,\vec{r}_3.....,\vec{r}_N)d\vec{r}_3.....d\vec{r}_N \quad \text{..... (14)}$$

Diagonal matrix element of the first-order density matrix is electron density

When $\vec{r}_1=\vec{r}_1'$, $\vec{r}_2=\vec{r}_2'$ eq.(13) turns into eq.(16)

$$\rho(\vec{r}_1)=\gamma_1(\vec{r}_1,\vec{r}_1)=N\int\psi^*(\vec{r}_1,\vec{r}_2,\vec{r}_3.....,\vec{r}_N)\psi(\vec{r}_1,\vec{r}_2,\vec{r}_3.....,\vec{r}_N)d\vec{r}_2d\vec{r}_3.....d\vec{r}_N \quad \text{..... (15)}$$

$$\rho_2(\vec{r}_1,\vec{r}_2)=\gamma_2(\vec{r}_1,\vec{r}_2,\vec{r}_1,\vec{r}_2)=N(N-1)\int\psi^*(\vec{r}_1,\vec{r}_2,\vec{r}_3.....,\vec{r}_N)\psi(\vec{r}_1,\vec{r}_2,\vec{r}_3.....,\vec{r}_N)d\vec{r}_3.....d\vec{r}_N \quad (16)$$

Eq.(16) operate on $\int d\vec{r}_2$

$$\int\rho_2(\vec{r}_1,\vec{r}_2)d\vec{r}_2=(N-1)\rho_1(\vec{r}_1) \quad \text{..... (17)}$$

## 2-4 Kohn-Sham theory：

The basis for Density Functional Theory (DFT) is proved by Hohenberg and Kohn theorem[5], which is determined the ground-state electronic energy completely by the one electron density $\rho(\vec{r})$. There exists one-to-one correspond between the electron density of a system and the energy.[6] The goal of DFT is to connect the electron density with the energy.[7,8]

$E$ is the total energy expressed by the expectation value, which includes

electron kinetic energy $T$, nuclear-electron attraction $V_{ne}$ and electron-electron repulsion $V_{ee}$ .In eq.(18), the nuclear-nuclear repulsion is a constant.

$$E = \langle \psi | H_e | \psi \rangle = T + V_{ne} + V_{ee} \quad \text{..... (18)}$$

$$\rho_1(\vec{r}_1) \equiv \rho(\vec{r}) \quad \text{..... (19)}$$

DFT is based on the ground state energy in eq.(20)

$$E = \langle \psi | H_e | \psi \rangle \rightarrow E_{DFT}[\rho] \quad \text{..... (20)}$$

Following are three terms in total energy. Respectively, $T$ , $V_{ne}$ and $V_{ee}$ . In eq.(18), the nuclear-electron attraction is a sum of terms, each depending on one-electron coordinate. The electron-electron repulsion depends on two electron coordinates.



2-4-1 In general form[4]

Kinetic energy

$$T = -\frac{1}{2}\int \nabla^2_{r_1} \gamma(\vec{r}_1, \vec{r}_2')\Big|_{r_1 = r_1'} d\vec{r}_1 \quad \text{..... (21)}$$

Nucleus-electron Coulomb attraction energy

$$V_{ne} = -\sum_{\alpha=1}^{N_n} \int \frac{Z_\alpha \rho_1(\vec{r}_1)}{|\vec{r}_1 - \vec{R}_\alpha|} d\vec{r}_1 \quad \text{..... (22)}$$

Electron-electron repulsion energy, which will divide into two parts in Hartree-Fock theory, Coulomb and exchange parts, $J[\rho]$ and $\mathrm{K}[\rho]$. $V_{ee}$ combines two terms as correlation parts.

$$V_{ee} = \frac{1}{2}\int \frac{\rho_2(\vec{r}_1, \vec{r}_2)}{|\vec{r}_1 - \vec{r}_2|} d\vec{r}_1 d\vec{r}_2 \quad \text{..... (23)}$$

2-4-2 In the ground state form

When energy level in ground state, eq.(21) will lead to eq.(24), eq.(22) will lead to eq.(27) and so on eq.(23) will lead to eq.(29). $T_s[\rho]$ is the exact kinetic energy by assuming non-interacting, and $T_s[\rho]$ is in Slater determinant composed of molecular orbital , $\phi_a$ .

Kinetic energy

$$T = -\frac{1}{2}\int \nabla^2_{r_1} \gamma(\vec{r}_1, \vec{r}_2')\Big|_{r_1=r_1'} d\vec{r}_1 \rightarrow T[\rho] = T_s[\rho] + (T[\rho] - T_s[\rho]) \quad \text{..... (24)}$$

$$T_s = \sum_{\alpha}^{N} \langle \phi_a | -\frac{1}{2}\nabla^2 | \phi_a \rangle \quad \text{..... (25)}$$

$$T_s[\rho] = \int \psi^*{}_s(\vec{r}_1, \vec{r}_2, \vec{r}_3, ..., \vec{r}_N)(-\frac{1}{2})(\sum_{i=1}^{N} \int \nabla_i{}^2)\psi_s(\vec{r}_1, \vec{r}_2, \vec{r}_3, ..., \vec{r}_N) d\vec{r}_1 d\vec{r}_2 ... d\vec{r}_N$$

$$= -\frac{1}{2}\sum_{\alpha} \int \phi_a{}^*(\vec{r})\nabla^2 \phi_a(\vec{r}) d\vec{r} \quad \text{..... (26)}$$

Where $T[\rho] - T_s[\rho]$ implies the kinetic correlation energy.

Nucleus-electron Coulomb attraction energy

$$V_{ne} = -\sum_{\alpha=1}^{N_n} \int \frac{Z_\alpha \rho_1(\vec{r}_1)}{|\vec{r}_1 - \vec{R}_\alpha|} d\vec{r}_1 \rightarrow E_{ne}[\rho] = -\sum_{\alpha=1}^{N_n} \int \frac{Z_\alpha \rho(\vec{r})}{|\vec{r} - \vec{R}_\alpha|} d\vec{r} \quad \text{..... (27)}$$

$$E_{ne}[\rho] = \int v_{ext}(\vec{r})\rho(\vec{r}) d\vec{r} \quad \text{..... (28)}$$

$$v_{ext}(\vec{r}) = -\sum_{\alpha=1}^{N_n} \frac{Z_\alpha}{|\vec{r} - \vec{R}_\alpha|} \quad \text{..... (29)}$$

$$v_{ext}(\vec{r}) = \varepsilon_{ext} \quad \text{..... (30)}$$

$\varepsilon_{ext}$ implies the external potential per electron.

Electron-electron repulsion energy

$$V_{ee} = \frac{1}{2}\int \frac{\rho_2(\vec{r}_1, \vec{r}_2)}{|\vec{r}_1 - \vec{r}_2|} d\vec{r}_1 d\vec{r}_2 \rightarrow E_{ee}[\rho] = J[\rho] + (E_{ee}[\rho] - J[\rho]) \quad \text{..... (31)}$$

Electron-electron Coulomb interaction energy

$$J[\rho] = \frac{1}{2}\int \frac{\rho(\vec{r})\rho(\vec{r}')}{|\vec{r} - \vec{r}'|} d\vec{r} d\vec{r}' \quad \text{..... (32)}$$

$(E_{ee}[\rho] - J[\rho]) = E_{xc}[\rho]$ is the electron exchange-correlation energy which is a rather small fraction of the total energy and the only unknown terms. In order to solve the exchange-correlation term needs lots of approximations.

$$E_{DFT}[\rho] = T_s[\rho] + E_{ne}[\rho] + J[\rho] + E_{xc}[\rho] \quad \text{..... (33)}$$

In eq.(33), $E_{xc}[\rho]$ is the unknown part, the other terms are already known.

$$E_{xc}[\rho] = (T[\rho] - T_s[\rho]) + (E_{ee}[\rho] - J[\rho]) \equiv \int \varepsilon_{xc}[\rho]\rho(\vec{r}) d\vec{r} \quad \text{..... (34)}$$

$E_{xc}[\rho]$ is the exchange-correlation energy; $\varepsilon_{xc}[\rho]$ is the exchange-correlation energy per electron. $(T[\rho] - T_s[\rho])$ is considered as the kinetic correlation energy. $E_{ee}[\rho] - J[\rho]$ contains potential correlation and exchange energy.

Furthermore,

$$E_{xc}[\rho] = E_x[\rho] + E_c[\rho] = \int \rho(\vec{r})\varepsilon_x[\rho(\vec{r})] d\vec{r} + \int \rho(\vec{r})\varepsilon_c[\rho(\vec{r})] d\vec{r} \quad \text{..... (35)}$$

$E_x[\rho]$ is a pure exchange part, $E_c[\rho]$ is a correlation part. $E_{xc}[\rho]$ has physical meaning.

## 2-5 Exchange-correlation energy

### 2-5-1 Local Density Approximation (LDA)：

$$v_{xc}(\vec{r}) = \varepsilon_{xc}(\vec{r}) + \int \frac{\delta\varepsilon_{xc}(\vec{r}')}{\delta\rho(\vec{r}')}\rho(\vec{r}')d\vec{r}' \quad \text{..... (36)}$$

When eq.(35) is only considered first term, eq.(36) it is assumed the density locally as slowly varying function.

$$v_{xc}(\vec{r}) = \varepsilon_{xc}(\vec{r}) \quad \text{..... (37)}$$

The exchange energy for a uniform electron gas is given by the Dirac formula

$$E_x^{LDA}(\rho) = -C_x \int \rho^{\frac{4}{3}}(r)dr \quad \text{..... (38)}$$

$$\varepsilon_x^{LDA} = -C_x \rho^{\frac{1}{3}} \quad \text{..... (39)}$$

2-5-2 General Gradient Approximation (GGA)[3]：

When eq.(35) is considered about higher correlation, the exchange and correlation energies depend on both electron density and derivatives of the density.

$$\frac{\delta\varepsilon_{xc}(\vec{r}')}{\delta\rho(\vec{r}')} \approx f(\rho, \nabla\rho) \quad \text{..... (40)}$$

2-5-3 Meta-GGA methods (meta-GGA)：

When eq.(37) is considered about higher order gradient correlation, it is with the Laplacian ($\nabla^2\rho$) as the second order term.

$$\frac{\delta\varepsilon_{xc}(\vec{r}')}{\delta\rho(\vec{r}')} \approx f(\rho, \nabla\rho, \nabla^2\rho) \quad \text{..... (41)}$$

2-6 Methods for finding reaction pathways between two stable states

The following methods (SPW and NEB) connect the reactant and product in the reaction of the images or structures and lead to the saddle point and to an approximation of the whole reaction path. The reaction path is based on reaction coordinate acting from reactant to product along a minimum energy

path (MEP).

2-6-1 Self-Penalty Walk (SPW) methods

In this method, the approximation reaction path is minimized by the average energy along the path, which is given as a line integral between reactant (R) and product (P). The line integral is approximation as a finite sum of M points. M is in the order of 10~20.

$$T(R,P)=\frac{1}{L}\int_{R}^{P}U(x)ds(x)\approx\frac{1}{L}\sum_{i=1}^{M}U(x_i)\Delta s_i(x) \quad \text{..... (42)}$$

$$T_{SPW}(R,x_2,x_3,...x_{M-1},P)=\frac{1}{L}\sum_{i=1}^{M}U(x_i)\Delta s_i(x)+\gamma\sum_{i=1}^{M-1}(d_{i,i+1}-\bar{d})^2+\rho\sum_{i>j+1}^{M-1}(-\frac{\mathrm{d_{ij}}}{\lambda\bar{\mathrm{d}}}) \quad \text{..... (43)}$$

$$d_{ij}=\left|x_i-x_j\right| \quad \text{..... (44)}$$

$$\bar{d}=\sqrt{\frac{1}{M+1}\sum_{i=1}^{M-1}d_{i,i+1}} \quad \text{..... (45)}$$

There are $\gamma$, $\lambda$ and $\rho$ parameters in the $T_{SPW}$ to find the suitable reaction path .The transition state (TS) is the point with the highest energy after minimization of the function $T_{SPW}$.

2-6-2 Nudged Elastic Band (NEB) methods：

The transition state is based on transition state theory at the maximum of MEP. Nudged Elastic Band (NEB) is modified versions of SPW. The Nudged Elastic Band method defines as the sum of energies and adds a penalty term having the purpose of distributing the points along the path.[9]A single spring constant $k$ will distribute images along the reaction path.

$$T_{NEB}(R,x_2,x_3,...,x_{M-1},P)=\sum_{i=1}^{M}U(x_i)+\frac{1}{2}\sum_{i=1}^{M-1}k(x_{i,i+1}-x_i)^2 \quad \text{..... (46)}$$

When $k$ is too large, $T_{NEB}$ will lead to cutting corners; when $k$ is too small, $T_{NEB}$ will lead to sliding down. In the Climbing Image (CI-NEB) version, one of the images is allowed to move along the elastic band to become the exact saddle point.[10] In our VASP calculation is constructed on CI-NEB methods. We have to decide how many middle points to set in $(x_2, x_3, ..., x_{M-1})$ on the reaction path.

## 2-7 Reference


(1) Kresse, G.; Furthmuller, J. *Vienna Ab-initio Simulation Package VASP the guide*, 2005.

(2) Segall, M. D.; Lindan, P. J. D.; Probert, M. J.; Pickard, C. J.; Hasnip, P. J.; Clark, S. J.; Payne, M. C. *Journal of Physics-Condensed Matter* **2002**, *14*, 2717.

(3) Perdew, J. P.; Burke, K.; Ernzerhof, M. *Physical Review Letters* **1996**, *77*, 3865.

(4) Zhu, C. Lecture Note in Quantum Computational Chemistry, 2007.

(5) Hohenberg, P.; Kohn, W. *Phys. Rev. B* **1964**, *136*, 864.

(6) Jensen *Introduction to Computational Chemistry*.

(7) Koch, W.; Holthausen, M. C. *A Chemist's Guide to Density Functional Theory* Wiley-VCH 2000.

(8) Koch, W.; Sham, L. J. *Phys. Rev. A* **1965**, *140*, 1133.

(9) Henkelman, G.; Jónsson, H. *J. Chem. Phys.* **2000**, *113*, 9978.

(10) Henkelman, G.; Uberuaga, B. P.; Jónsson, H. *J. Chem. Phys.* **2000**, *113*, 9901.

# Chapter Three

# Results and Discussion

## 3-1 Verification

In the following calculations, the slab model is applied, respectively, to study the interaction between nitric acid and the $TiO_2$ rutile (110) surface as well as nitric acid and the anatase (101)[1] surface. The slab cell constructed for the $TiO_2$ rutile and anatase calculations includes 16 $TiO_2$ as a unit cell shown in Figure 3-1-1(a), 3-1-1(b), 3-1-1(c) and 3-1-1(d). All slabs are separated by a vacuum space of greater than 13.0 Å is employed in the direction parallel to the <110> and <101> coordinate, respectively. This large separation is used to avoid the interaction force between the upper and lower slabs. The whole layers of the super cell are not fixed in the following calculations in order to simulate with good accuracy.

The parameters are set for the $TiO_2$ rutile (110) and anatase (101) surfaces with cut off energy (Ecut) equal to 600 eV to include kinetic energies ($\frac{\hbar^2 k^2}{2m}$) in the basis set. The cut-off energy is bigger than real kinetic energies in a convergent system. The Monkhorst-Pack k-points are based on the Brillouin zone which is chosen by 4x4x1 in rutile and 4x5x1 in anatase. The parameters set in the cut-off energy and k-point are useful to help the convergence of a system.

Similar parameters were set in gas molecule simulations, but we allow Monkhorst-Pack k-points to 1x1x1. Gas-phase atoms and molecules were separated by 15Å as vacuum space, which is simulated with a quantum cubic box with sides 15Å. The sufficiently large size vacuum space reduces interaction between neighboring systems.

The parameters set in transition state[2] calculations respectively are ISPRING=-5, IBRION=1 and LCLIMB[3]=.True. IBRION=1 means to find local minimum, respectively. We utilize the climbing-image nudged-elastic band (CI-NEB)[3] to achieve a bigger accuracy.

The adsorption energy, $E_{ads}$ is computed according to equation (46):

$$E_{ads} = -[E_{total} - (E_{slab} + E_{molecule})] \quad \text{..... (46)}$$

Where $E_{slab}$ indicates the energy of the clean slabs or surface, $E_{molecule}$ is the energy of a gas-phase molecule, $E_{total}$ is the total energy of adsorbed species on the surface. The surface energy is considered for the $TiO_2$ surface with a hydrogen adsorbed on it, the adsorption energy is calculated as follows:

$$E_{ads} = -[E_{total/H} - (E_{slab/H} + E_{molecule})] \quad \text{..... (47)}$$

Where $E_{slab/H}$ indicates the energy of the slab with an H atom adsorbed on the slab, and $E_{total/H}$ is the total energy of the slab with the adsorbate and H co-adsorbed on it. The spin-polarized effect is insignificant, because the difference in the adsorption energy is merely +0.05 kcal/mole with the spin-polarized parameter.

A positive value of $E_{ads}$ >0 suggests a stable adsorption. Analysis on atomic charges of optimized structures is calculated by utilizing the Bader method with a program designed by Henkelman et al.[4] With the program, we can analyze the data with the detail in the charge transfer between an adsorbate and the surface.

### 3-1-1 $TiO_2$ rutile(110) and anatase(101) surface

In our calculations of the $TiO_2$ rutile (110) surface, we use 1x2x2 super

cell for $HNO_3$ monomer/$TiO_2$ system shown in Figure 3-1-1(a) and 1x4x1 super cell shown for $HNO_3$ dimer/$TiO_2$ system in Figure 3-1-1(b) with $Ti_{16}O_{32}$. The surface sizes are 6.495 Å x 5.866 Å and 6.495 Å x 11.732 Å, respectively. We use two kinds of the $TiO_2$ rutile surface to avoid the interaction of large-size molecules with each other. We utilize two sizes of the anatase surface for the same reason.

For the anatase surface, the models used are the 2x1x2 super cell shown in Figure 3-1-1(c) for $HNO_3$ monomer/$TiO_2$ system and 3x1x2 super cell for dimer $HNO_3$/$TiO_2$ system shown in Figure 3-1-1(d). In the 2x1x2 super cell with $Ti_{16}O_{32}$, the size of the surface is 7.57 Å x 10.239 Å. In the 3x1x2 super cell with $Ti_{24}O_{48}$ composition, the surface is 11.355 Å x 10.239 Å.

To ensure the reliability of the computational results, we first compared the calculated bulk lattice constants. The predicted lattice constants are a = 4.593 Å and c = 2.933 Å for rutile and a = 3.785 Å and c = 10.239 Å for anatase which are in good agreement with the experimental values of a = 4.594 Å and c = 2.958 Å for rutile[5] and a = 3.782 Å and c = 9.502 Å for anatase[6], respectively. The optimized geometries of $HNO_3$ and $NO_3$ are shown in Figure 3-1-1(e) and Figure 3-1-1(f).

Figures 3-1-1(a) and 3-1-1(c) show different adsorption sites which have been labeled on the $TiO_2$ surface. They are five-fold coordinated titanium, six-fold coordinated titanium, two-fold bridging oxygen, and three-fold coordinated oxygen, corresponding to $Ti_{5c}$, $Ti_{6c}$, $O_{2c}(O_b)$, and $O_{3c}$, respectively. The twofold coordinated O atoms and fivefold coordinated Ti atoms are more active than the threefold O atoms and the sixfold coordinated Ti atom, respectively, due to their unsaturated coordinations. On rutile surface, the bond lengths of $Ti_{5c}$-$Ti_{5c}$, $Ti_{5c}$-$O_{3c}$ are 2.933Å and 1.817Å, respectively. The angle of

$Ti_{5c}$-$O_{2c}$-$Ti_{5c}$ is 106.5°, which may be compared with those of Huang, et al.[7], the bond lengths of $Ti_{5c}$-$Ti_{5c}$, $Ti_{5c}$-$O_{3c}$ are 2.974 Å, 1.819Å and the angle of $Ti_{5c}$-$O_{2c}$-$Ti_{5c}$ is 108.2°, respectively.

### 3-1-2 Testing the Model with $H_2O$ adsorption

The test models have been compared with the adsorption energies of $H_2O$[8,9] on the surface. The $H_2O$-rutile and $H_2O$-anatase adsorption structures are shown in Figures 3-1-2 (a), 3-1-2(b) and Table 3-1-2(a), 3-1-2(b), 3-1-2(c).

*Adsorption of $H_2O$:*

As shown in the Figure 3-1-2 (a), the most stable structure $H_2O$-$Ti_{5c}$-up/para (a) for the $H_2O$-$TiO_2$ rutile system among the six kinds of adsorption configurations is with one hydrogen bonding to the nearest bridged oxygen. The most stable structure is $H_2O$-$Ti_{5c}$-paraleft (a) for the $H_2O$-$TiO_2$ anatase system. The adsorption energies on the rutile and anatase surfaces are 16.6 kcal/mol and 15.7 kcal/mol, respectively, which are close to the result of another theoretical calculation 18.9 kcal/mole[7] on the rutile and 19.2 kcal/mol[8] on the anatase surfaces, indicating the adsorption of $H_2O$ on the $Ti_{5c}$ with an H atom tilting forward to the bridged surface oxygen. Herman et al.[10] in an experimental investigation show the adsorption of $H_2O$ on the rutile surface is slightly higher than that on the anatase surface; the adsorption energies are from 0.74eV to 0.72 eV (17.1 kcal/mol to 16.6 kcal/mol) for the $H_2O$ adsorbed on the anatase surface and from 0.74 eV to 0.64 eV (17.1 kcal/mol to 14.8 kcal/mol) for the $H_2O$-ruilte system due to different water coverages. Our calculated values are in very good with the experimental values[10]. Other structure ($H_2O$-$O_{2c}$-down (a)) with small adsorption energies of 2.3 kcal/mol on the rutile surface and 1.9 kcal/mol on the anatase surface are physisorbed states

without direct interactions with $Ti_{5c}$ atoms.

## 3-2 Adsorption and reaction mechanism of $HNO_3$ and $HNO_3$ dimer on $TiO_2$ surface

### 3-2-1 Adsorption of $HNO_3$ and $NO_3$ on rutile $TiO_2$ (110)

*Adsorption of $HNO_3$:*

In our study, the adsorption of nitric acid was found to have four different configurations on different sites of the metal oxide surface ($Ti_{5c}$, $O_{3c}$). These adsorption configurations and their fragments on the $TiO_2$ rutile (110) surface are shown in Figure 3-2-1(a), and the associated bond lengths and adsorption energies are listed in Table 3-2-1(a).

In these four types of structures, the most stable one is a molecular configuration with an oxygen attached to the surface $Ti_{5c}$ atom and the hydrogen formed a hydrogen bond with the nearest bridge oxygen on the surface indicated by $Ti_{5c}$-ON(O)OH…$O_{2c}$(a). Its adsorption energy is 6.7 kcal/mol and the $Ti_{5c}$-O bond length is 2.428 Å and $O^3H^1$-$O_{2c}$ is 2.288 Å as listed in Table 3-2-1(a). Although the adsorption energies of the exhibited four structures are not big enough to stabilize $HNO_3$ for a long time, $Ti_{5c}$-ON(O)OH…$O_{2c}$(a) shows clearly that the formation of a hydrogen bond can increase the adsorption energy.

*Adsorption of $NO_3$:*

We obtain two different configurations of ON(O)O on the rutile surface as shown in Figure 3-1-2(a); one is $Ti_{5c}$-ON(O)O-$Ti_{5c}$(a) with two oxygen atoms bonding with $Ti_{5c}$ atoms on the surface and the other is $Ti_{5c}$-ON(O)O-$Ti_{5c}$-2(a) with one oxygen on a $Ti_{5c}$ atom. The adsorption energy of the former is 12.0 kcal/mol, and that of the latter is 4.7 kcal/mol. Thus the formation of the O-$Ti_{5c}$ bond can stabilize the structure with a higher adsorption energy.

### 3-2-2 Adsorption of $HNO_3$ and $NO_3$ on $TiO_2$ (101) anatase

For the $HNO_3$-anatase system, we utilize a 3x1x2 super cell with $Ti_{16}O_{32}$.

*Adsorption of $HNO_3$:*

We obtain three types of $HNO_3$ adsorption configurations on the $TiO_2$ anatase (101) surface as shown in Figure 3-2-1(b) and the bond length and adsorption energies are shown in Table 3-2-2(a). The most stable structure is similar to that on the rutile (110) surface with the configuration $Ti_{5c}$-ON(O)OH-$O_{2c}$(a), having a hydrogen bond involving the H atom and the nearest neighboring oxygen site. Its adsorption energy is 13.3 kcal/mol. The other configurations of $HNO_3$, with two oxygen atoms connecting to $Ti_{5c}$ atoms on the surface are less stable than the hydrogen-bonded structure, the $Ti_{5c}$-ON(O)OH-$O_{2c}$(a).

*Adsorption of $NO_3$:*

In Figure 3-2-2(a), we have two structures of $NO_3$ adsorbed on the anatase surface. The adsorption energy of $Ti_{5c}$-ON(O)O-$Ti_{5c}$(a) is 6.6 kcal/mol and that of $Ti_{5c}$-ON(O)O-$Ti_{5c}$-2(a) is 5.6 kcal/mol. The bond lengths of $Ti_{5c}$-$O^1$ in $Ti_{5c}$-ON(O)O-$Ti_{5c}$(a) and $Ti_{5c}$-ON(O)O-$Ti_{5c}$-2(a) are 2.259Å and 3.203Å, respectively. The bond length of $Ti_{5c}$-O is shorter, and the adsorption energy is higher.

### 3-2-3 Reaction path for the adsorption and dissociation of $HNO_3$ on the rutile (110) surface

The potential energy surface of dissociative adsorption reactions of nitric acid on the clean rutile (110) surface is shown in Figure 3-2-3. The optimized structures are shown in Figure 3-2-1(a) and bond lengths are indicated in Table 3-2-1(a). From the prior calculation, the most stable adsorption configuration is

considered. First, nitric acid on the clean rutile (110) surface is a monodentate structure with the hydrogen bond formed with the nearest neighboring bridging oxygen with an adsorption energy of 6.7 kcal/mol. In the dissociation process, the hydrogen atom can migrate to the neighboring $O_{2c}$ forming $Ti_{5c}$-ON(O)O...H-$O_{2c}$(a); the reaction is slightly exothermic and occurs without a well-defined transition state. Second, the adsorbed $NO_3$ (a) can molecularly rotate on the surface. The rotation of the adsorbate $Ti_{5c}$-ON(O)O... H-$O_{2c}$(a) resulting in the formation of a covalently bond $Ti_{5c}$-ON(O)O-$Ti_{5c}$,H-$O_{2c}$(a) as shown in Figure 3-2-1(a). This rotation reaction has an activation barrier lying 3.3 kcal/mole above the reactants. The calculated activation barrier above the adsorbate is 12.2 kcal/mol. The isomerization process from $Ti_{5c}$-ON(O)O...H-$O_{2c}$(a) to $Ti_{5c}$-ON(O)O-$Ti_{5c}$,H-$O_{2c}$(a) is calculated to be exothermic by 7.6 kcal/mol. The transition state (TS1) of this process shown in Figure 3-2-7 and Table 3-2-3 corresponds to the formation of the $Ti_{5c}$-$O^1$ with a bond length of 2.187 Å and the formation of the $O_{2c}$-$H^1$ with 0.969 Å. According to the previous calculation, eliminating the $NO_3$ gas molecule from $Ti_{5c}$-ON(O)O-$Ti_{5c}$,H-$O_{2c}$(a) to produce H-$O_{2c}$(a) + $NO_3$(g) requires 58.7 kcal/mol which implies that the adsorption process can not occur spontaneously.

On the other hands, $NO_3$ (a) can more easily split into $NO_2$ (a) + O (a) by breaking one of the N-O bonds, which is endothermic by about 22.1 kcal/mol.

### 3-2-4 Reaction path for the adsorption and dissociation of $HNO_3$ on the anatase (101) surface

The computed potential energy surface for the dissociative adsorption reaction of $HNO_3$ on the clean anatase (101) surface is shown in Figure 3-2-4.

The energies are all referenced to the initial reactants, $HNO_3$ + $TiO_2$ anatase (101) surface. The optimized structures with the surface model are depicted in Figure 3-2-2(a) and the selected bond lengths are presented in Table 3-2-2(a). First, we consider the most stable adsorption configuration, $Ti_{5c}$-ON(O)OH-$O_{2c}$(a). The hydrogen of the coordinating $O^3H^1$ group can migrate to the neighboring $O_{2c}$ to form $Ti_{5c}$-ON(O)O…H-$O_{2c}$(a) which is slightly exothermic by 0.4 kcal/mol. The phenomenon of hydrogen migrating is same as that in the rutile (110) surface. The bond length of $Ti_{5c}$-$O^1$ is 2.027 Å. The adsorbed ON(O)O molecule can rotate on the surface to form $Ti_{5c}$-ON(O)O-$Ti_{5c}$,H-$O_{2c}$(a). The rotation requires 1.6 kcal/mol energy and the bond length between Ti-O is increased by 0.12 Å. The rotation of ON(O)O molecule in the adsorbate $Ti_{5c}$-ON(O)O-$Ti_{5c}$,H-$O_{2c}$(a) can result in the formation of two Ti-O bonds on two $Ti_{5c}$ sites with the bond lengths of $Ti_{5c}$-$O^1$ and $Ti_{5c}$-$O^3$, 2.143 Å and 2.159 Å, respectively. In the isomerization process from $Ti_{5c}$-ON(O)…H-$O_{2c}$(a) to $Ti_{5c}$-ON(O)O-$Ti_{5c}$,H-$O_{2c}$(a), it has to overcome an activation barrier of 9.1 kcal/mol at TS3, which is below the reactant by 4.6 kcal/mol in energy. In the transition state (TS3) shown in Figure 3-2-7 and Table 3-2-3, the bond lengths of $Ti_{5c}$-$O^1$ and $Ti_{5c}$-$O^3$ are 2.002 Å and 3.027 Å, respectively. The decomposition process producing H-$O_{2c}$(a) + $NO_3$(g) from $Ti_{5c}$-ON(O)O-$Ti_{5c}$,H-$O_{2c}$(a) requires 56.8 kcal/mol and the final product H-$O_{2c}$ + $NO_3$(g) is 44.7 kcal/mol above the initial reactants.

### 3-2-5 Reaction path for the adsorption and dissociation of $HNO_3$ dimer on the rutile(110)surface

The geometrical structures and potential energy surface of dimer $HNO_3$ molecules on the $TiO_2$ rutile (110) surface are shown in Figure 3-2-1(b) and

Figure 3-2-5. The corresponding bond lengths and adsorption energies are listed in Table 3-2-1(b). In the dimer $HNO_3$ adsorption on the rutile surface, we use 1x4x1 super cell as our $TiO_2$ rutile (110) model. The difference between 1x2x2 and 1x4x1 that is the latter has 2 times higher width with half of the height of the former.

In the reaction path, we only consider the most stable structure of $HNO_3$ dimer as given for the monomer $HNO_3$ adsorption with an adsorption energy of 12.8 kcal/mol, approximately twice that of the monomer. In the most stable conformation, two $HNO_3$ molecules adsorbed parallel to each other on two surface $Ti_{5c}$ atoms, having two hydrogen bonds formed with the closest neighboring bridged oxygen $O_{2c,}$ depicted as 2($Ti_{5c}$-ON(O)OH-$O_{2c}$(a)) in Figure 3-2-2(b). Their bond lengths are $Ti_{5c}$-$O^1$=2.594 Å, $Ti_{5c}$-$O^4$=2.551 Å and $O^3H^1$=2.266 Å, $O^3H^1$=2.163 Å.

Starting from the most stable adsorbate 2($Ti_{5c}$-ON(O)OH-$O_{2c}$(a)), the $H^1O^3$-$N^1$ bond of one $HNO_3$ molecule rotates and forms a hydrogen bond with another $HNO_3$ giving intermediate LM1, whose adsorption energy is higher than that of 2($Ti_{5c}$-ON(O)OH…$O_{2c}$(a)) by 5.1 kcal/mol. In the intermediate LM1, the intermolecular hydrogen bond length is 2.203 Å between the $H^2$ atom and the $O^3H^1$ of the first $HNO_3$. This finding is consistent with the results reported by M. J. Gillan[11] who have showed the intermolecular hydrogen bonding can stabilize the configuration. From the intermediate, the H atom of the first $HNO_3$ split to form $H_2O$ with the OH group of the second $HNO_3$ via TS2, producing a water complex $Ti_{5c}$-ON(O)ON(O)O-$Ti_{5c}$,$O_{2c}$…HOH…$O_{2c}$(a). The process demands 46.2 kcal/mol for crossing the barrier. From the water complex, it can eliminate the $H_2O$(g) from the surface to form a $Ti_{5c}$-ON(O)ON(O)O-$Ti_{5c}$(a) + $H_2O$(g)

with 5.8 kcal/mol endothermicity. The adsorption energy of $Ti_{5c}$-ON(O)ON(O)O-$Ti_{5c}$(a) is not big enough to stabilize the structure on $TiO_2$.

Furthermore, the $N_2O_5$ molecule adsorbed on the rutile surface have two different structures shown in Figure 3-2-1(b). The adsorption energies of $Ti_{5c}$-ON(O)ON(O)O-$Ti_{5c}$(a) and $Ti_{5c}$-ON(O)ON(O)O-$Ti_{5c}$-2(a) are 2.0 kcal/mol and 1.5 kcal/mol, respectively. These structures are not stable enough to form $N_2O_5$(a). $Ti_{5c}$-ON(O)ON(O)O-$Ti_{5c}$(a) easily splits into $NO_3$ and $NO_2$ molecules without a well-defined transition state. The final product of $NO_3$ and $NO_2$ on the surface lies 3 kcal/mol below $Ti_{5c}$-ON(O)ON(O)O-$Ti_{5c}$(a).

### 3-2-6 Reaction path for the adsorption and dissociation of $HNO_3$ dimer on the anatase (101) surface

Similarly, Figure 3-2-6 shows the potential energy diagrams and Figure 3-2-2(b) shows the related geometrical structures of $HNO_3$ dimer on the $TiO_2$ anatase (110) surface. For this process, we utilize 3x1x2 super cell with the 11.355Å x12.289 Å area on the $TiO_2$ (101) anatase surface. For the $HNO_3$ dimer adsorbed on a smaller 2x1x2 super cell, there is unavoidable interaction between the cells. The related bond lengths and the adsorption energies are presented in Table 3-2-2(b). We consider the most stable configuration $Ti_{5c}$-ON(O)OH…$O_{2c}$(a) given in the Figure 3-2-2(a) which has an adsorption energy of 13.3 kcal/mol. Thus, the most stable $HNO_3$ dimer is 2($Ti_{5c}$-ON(O)OH…$O_{2c}$(a)) with the adsorption energy 28.3 kcal/mol, which is approximately twice that of the monomer $Ti_{5c}$-ON(O)OH-$O_{2c}$(a). In the most stable configuration, 2 $HNO_3$ molecules with oxygen atoms attaching to two

$Ti_{5c}$ atoms on the surface and with the two hydrogen atoms forming hydrogen bonds with the nearest two bridged oxygen atoms. Their bond lengths are $Ti_{5c}$-$O^1$ 2.309 Å, $Ti_{5c}$-$O^4$ 2.332 Å, $O^3H^1$-$O_{2c}$ 1.498 Å and $O^6H^2$-$O_{2c}$ 1.484 Å, respectively.

From the most stable dimer adsorbate 2($Ti_{5c}$-ON(O)OH-$O_{2c}$(a)), one of the H atoms can react with the OH group of the second $HNO_3$[11] to form $H_2O$ giving $Ti_{5c}$-ON(O)O-$Ti_{5c}$,$O_{2c}$…HOH…$O_{2c}$(a) via TS4 as shown in Figure 3-2-7. The transition state (TS4) is 40.0 kcal/mol higher than the initial reactants. The activation barrier for breaking the hydrogen bond requires 68.2 kcal/mol. The bond lengths of $O^3$-$H^1$ and $O^6$-$H^1$ are 1.873 Å and 3.120 Å. The $Ti_{5c}$-ON(O)O-$Ti_{5c}$,$O_{2c}$…HOH…$O_{2c}$(a) is 3.1 kcal/mol above the initial reactants. From $Ti_{5c}$-ON(O)O-$Ti_{5c}$,$O_{2c}$...HOH...$O_{2c}$(a), it can eliminate $H_2O$(g) to produce $Ti_{5c}$-ON(O)ON(O)O-$Ti_{5c}$(a) + $H_2O$ (g). The dehydration reaction requires 4.8 kcal/mol. Thus, $Ti_{5c}$-ON(O)O-$Ti_{5c}$,$O_{2c}$…HOH…$O_{2c}$(a) is not stable and can not retain $H_2O$ on the surface.

Moreover, the $N_2O_5$ molecules can adsorb on the anatase surface with two different structures as shown in Figure 3-2-2(b). The adsorption energies of $Ti_{5c}$-ON(O)ON(O)O-$Ti_{5c}$(a) and $Ti_{5c}$-ON(O)ON(O)O-$Ti_{5c}$-2(a) are 2.1 kcal/mol and 0.2 kcal/mol, respectively; they are too small for the $N_2O_5$ molecules to adsorb on the rutile surface.

## 3-3 Hydrogen effect on adsorbate structures and adsorption energies

In this section, we discuss the effect of H adsorbed on a neighboring oxygen ($O_{2c}$) in the nitric acid system. The adsorption energies on rutile and anatase are listed in Table 3-3(a) and Table 3-3(b), respectively. We will not take spin-polarization into consideration, because these are little change in

geometries and the difference in adsorption energies of nitric acid is no more than ± 0.1 kcal/mol. As discussed above, nitric acid adsorbed on clean $TiO_2$ rutile (110) surface has four different of structures. The most stable structure is $Ti_{5c}$-ON(O)OH…$O_{2c}$(a) with an adsorption energy of 6.7 kcal/mol. For the hydrogen bonding $O_{2c}$ atom, the bond lengths of $Ti_{6c}$-$O_{2c}$ are 1.855 Å and 1.838 Å. Table 3-3(a) indicates the co-adsorption of H on a neighboring oxygen in $Ti_{5c}$-ON(O)OH…$O_{2c}$(a) to produce $Ti_{5c}$-ON(O)O…H-$O_{2c}$(a) has a higher adsorption energy, 9.9 kcal/mol. The bond lengths of $Ti_{6c}$-$O_{2c}$ are 2.070 Å and 1.838 Å. Moreover, the co-adsorption of two hydrogen atoms on the two neighboring $O_{2c}$ will increase adsorption energy to 11.7 kcal/mol. The bond lengths of $Ti_{6c}$-$O_{2c}$ are 2.087 Å and 2.008 Å.

Similarly, nitric acid adsorbed on clean $TiO_2$ anatase has three different structures. The most stable one is $Ti_{5c}$-ON(O)OH…$O_{2c}$(a) with 13.3 kcal/mol adsorption energy. Comparing with one hydrogen adsorbed on a bridging oxygen, the adsorption energy is a bit lower than that of $Ti_{5c}$-ON(O)OH-$O_{2c}$(a), 10.5 kcal/mol. The bond lengths of $Ti_{6c}$-$O_{2c}$ are 2.220 Å and 1.917 Å. So with two hydrogen co-adsorbed on bridging oxygen atoms, the adsorption energy is slightly lower than the former, 8.9 kcal/mol. The bond lengths of $Ti_{6c}$-$O_{2c}$ are 2.242 Å and 2.190 Å.

The effect of hydrogen absorbed on a bridging oxygen results in increasing adsorption energy on the $TiO_2$ rutile (110) surface, but decreasing the adsorption energy on the $TiO_2$ anatase (101) surface. With the hydrogen on bridging oxygen leads the increase in the bond length of $Ti_{6c}$-$O_{2c}$ from 1.855 Å to 2.087 Å in the rutile (110) surface and from 1.936 Å to 2.242 Å in the anatase (101) surface.

In addition, we compare hydrogen effects on $Ti_{5c}$-ON(O)O-$Ti_{5c}$(a) and

$Ti_{5c}$-ON(O)O-$Ti_{5c}$,H-$O_{2c}$(a) on the rutile and anatase surfaces. The results are shown in Figure 3-4 and Table 3-3(c). The adsorption energies with hydrogen attaching to the neighboring bridged oxygen on the rutile surface is 58.7 kcal/mol and that without hydrogen is 12.0 kcal/mol. On the anatase surface, the adsorption energy with and without hydrogen on the bridged oxygen are 56.7 kcal/mol and 6.6 kcal/mol, respectively. In order to explain the hydrogen effect on the adsorption energy, we analyze the Bader charges of $Ti_{5c}$-ON(O)O-$Ti_{5c}$(a) and $Ti_{5c}$-ON(O)O-$Ti_{5c}$,H-$O_{2c}$(a) on both surfaces.

## 3-4 Bader atomic charges

We calculate the Bader charges for the adsorbate ON(O)O on the $TiO_2$ rutile(110) and anatase (101) surfaces with and without an H atom co-adsorbated on the bridging oxygen as shown in Figure 3-4.

In the rutile (110) surface, H atom co-adsorption increases the charge of the ON(O)O adsorbate by 0.21 e, where e is the magnitude of the charge of the electron. In Figure 3-4, the charge of the bridged surface oxygen with an H atom is -1.45 e and the H atom is 1.00 e. Comparing with to the bridged surface oxygen without H, it is -0.82 e.

Similarly, in the anatase (101) surface, H atom adsorption on the bridged oxygen with the ON(O)O adsorbate increases the charge by 0.22 e. The charge of the bridged oxygen with H atom is -1.35 e and the H atom is 0.86 e. Without co-adsorbed H atom the charge is -0.84 e. This phenomenon suggests that an H atom on the bridged oxygen will distribute its atomic charge in the adsorbate and stabilize the configuration with a higher adsorption energy as listed in Table 3-3(c), in which the difference with and without a co-adsorbed H atom is 46.7 kcal/mol on the $TiO_2$ rutile (110) surface, and 50.13 kcal/mol in

the $TiO_2$ anatase (101) surface. The results of the Bader charge analysis on the rutile surface are consistent with those on the anatase surface. The hydrogen effect on $NO_3$ adsorbate is a significant difference in the adsorption energy due to the charge transfer from surface to $NO_3$.

### 3-5 $(InN)_x$, x=1, 2, 3, 6, 10

The topic is about $(InN)_x$ clusters with nitric acid as a linker adsorbing on $TiO_2$ rutile(110) and anatase(101) surfaces. To understand the charge transfer phenomenon and the adsorption energy of $(InN)_x$, we computationally study these systems with VASP.

The adsorption energies and bond lengths of $(InN)_x$, x=1, 2, 3, 6, 10, each connecting with an adsorbed $NO_3$ are listed the Table 3-5(a) and Table 3-5(b) for the rutile and anatase surfaces, respectively.

On the rutile surface, the $(InN)_x$, x=1, 3 adsorbed on $NO_3$ with an H atom co-adsorbed on a bridged oxygen is shown in Figure 3-5-1(a). The $(InN)_x$, x=1, the In-N-O is linear and the $In^1$-$O^2$ bond length is 2.180 Å. The adsorption of (InN)-ON(O) on the rutile surface is merely 8.3 kcal/mol. When $(InN)_x$, x=2, the configuration of $(InN)_2$-ON(O)O is not sufficiently stable to maintain the $(InN)_2$ structure on the $TiO_2$ rutile(110) surface. $(InN)_2$ easily emits $N_2$ gas. For $(InN)_x$, x=3, the $(InN)_3$ molecule has two kinds of hexagon structures, one with $In^1$-$O^2$ bond length with 2.232 Å and the other with 2.347 Å. For the non-symmetric $(InN)_3$ adsorbate, $(InN)_3$-ON(O)O-$Ti_{5c}$, its adsorption energy is higher than that of the symmetric $(InN)_3$-ON(O)O-$Ti_{5c}$-2 by 9.8 kcal/mol. In the case of $(InN)_x$, x=6 and 10 with a wurtzite cluster structure, the adsorption energies are 14.8 kcal/mol and 50.2 kcal/mol, respectively.

On the anatase surface, the similar structures of $(InN)_x$, x=1 and 3, have

adsorption energy 14.5 kcal/mol for (InN)-ON(O)O and 45.4 kcal/mol and 34.6 kcal/mol for $(InN)_3$-ON(O)O due to two different configurations as alluded to above for the analogous with surface. The adsorption energies of $(InN)_6$ and $(InN)_{10}$ on $TiO_2$ anatase are 10.7 kcal/mol and 48.2 kcal/mol, respectively, without the ON(O)O linker.

### 3-6 Bader Charge analysis of $(InN)_x$, x=1, 2, 3, 6, 10

The analyses the charges of $(InN)_x$-ON(O)O(a), x=1, 2, 3, 6, 10 with an H atom co-adsorbed on $TiO_2$ rutile(110) and anatase(101) are shown in Figures 3-5-1(a), 3-5-1(b) and 3-5-2(a), 3-5-2(b) and Table 3-6(a),3-6(b). The $Ti_{5c}$ atoms on the surface without the ON(O)O linker are 2.46 e and 2.46 e on the rutile and anatase surface, respectively. The two $Ti_{5c}$ atoms attached with ON(O)O molecules will increase their charges to 2.51 e and 2.50 e, and 2.53 e and 2.50 e, on the rutile and anatase surface, respectively. The charges of $Ti_{5c}$ atoms on both surfaces decrease to 2.48 e after $(InN)_x$, adsorption.

With the ON(O)O molecule adsorbing on the $TiO_2$ rutile and anatase surfaces, the charges of ON(O)O are -0.78 e on both surfaces. Following the attachment of $(InN)_x$, x=1, 2, 3, 6, 10, to ON(O)O, the charge distributions will increase the electron density to near the ON(O)O molecule side. Because the ON(O)O molecule is an electron withdrawing radical, it can easily attract more electrons, the $(InN)_x$ cluster will thus become more positive. Therefore, we may infer ON(O)O as a linker is not an enhancement in power conversion efficiency.

## 3-7 Reference


(1) Diebold, U. *Surface Science Reports* **2003**, *48*, 53.

(2) Eyring, H. *J. Chem. Phys.* **1935**, *3*, 107.

(3) Vasp TST Tools.

(4) Henkelman, G.; Arnaldsson, A.; Jónsson, H. *Computational Materials Science* **2006**, *36*, 354.

(5) Vinet, P.; Ferrante, J.; Smith, J.; Rose, J. *J. Phys. C* **1986**, *19*, L467.

(6) Burdett, J. K.; Hughbanks, T.; Miller, G. J.; Richardson Jr, J. W.; Smith, J. V. *Journal of the American Chemical Society* **1987**, *109*, 3639.

(7) Huang, W. F.; Raghunath, P.; Lin, M. C. *J. Comput. Chem* **2008**, communicated.

(8) Raghunath, P.; Lin, M. C. *J. Phys. Chem. C* **2008**, *112*, 8276.

(9) Vittadini, A.; Selloni, A.; Rotzinger, F. P.; Gräzel, M. *Physical Review Letters* **1998**, *81*, 2954.

(10) Herman, G. S.; Dohnalek, Z.; Ruzycki, N.; Diebold, U. *J. Phys. Chem. B* **2003**, *107*, 2788.

(11) Lindan, P. J. D.; Harrison, N. M.; Gillan, M. J. *Physical Review Letters* **1998**, *80*, 762.

# Chapter Four

# Conclusions

## 4 Conclusions

In summary, we perform systematic investigations on the $HNO_3$ adsorbed on the $TiO_2$ rutile (110) and anatase (101) surfaces by DFT calculations. The key conclusions are summarized as follows:

(1) The adsorption and reaction of the monomer nitric acid on the rutile (110) surface:

The most stable configuration for nitric acid on the clean rutile (110) surface is a monodentate structure with one hydrogen bonded to a neighboring bridging oxygen, its adsorption energy is 6.7 kcal/mol. The resulting $Ti_{5c}$-ON(O)OH...$O_{2c}$(a) can go over a small barrier for H atom migration to the bonding bridged oxygen forming a more stable $Ti_{5c}$-ON(O)O...H-$O_{2c}$(a) with an exothermicity of 8.9 kcal/mol. The rotation of ON(O)O adsorbate starting from $Ti_{5c}$-ON(O)O...H-$O_{2c}$(a) to form $Ti_{5c}$-ON(O)O-$Ti_{5c}$,H-$O_{2c}$(a) requires a barrier of 13.2 kcal/mol. Then, the elimination of $NO_3$ from $Ti_{5c}$-ON(O)O-$Ti_{5c}$,H-$O_{2c}$(a) to produce H-$O_{2c}$(a) + $NO_3$(g) has an endothermicity of 58.7 kcal/mol, which corresponds to the binding energy of $NO_3$ with the H-covered rutile $TiO_2$ surface.

(2) The adsorption and reaction of the dimer nitric acid on the rutile (110) surface:

In the case of $HNO_3$ dimer, two equivalent monodentate structures nitric acid 2($Ti_{5c}$-ON(O)OH…$O_{2c}$(a)) absorbed on two 5-fold coordinated Ti atoms of the rutile surface is the most stable configuration with an adsorption energy of

12.8 kcal/mol, which are slightly smaller than two times of the monodentate. The result indicates that the effect of adsorbate interaction is negligible. According to the PES shown in Figure 3-2-5, the intermediate LM1 is a local minimum with an exothermic energy of 17.8 kcal/mol. The dehydration process from LM1 to $Ti_{5c}$-ON(O)ON(O)O-$Ti_{5c}$,$O_{2c}$...HOH...$O_{2c}$(a) needs a high barrier of 46.2 kcal/mol. The $Ti_{5c}$-ON(O)ON(O)O-$Ti_{5c}$,$O_{2c}$...HOH...$O_{2c}$(a) can barrierlessly eliminate the $H_2O$ molecule dissociate to produce $Ti_{5c}$-ON(O)ON(O)O-$Ti_{5c}$(a) + $H_2O$(g) with a small endothermicity of 5.8 kcal/mol.

(3) The adsorption and reaction of the monomer nitric acid on the anatase (101) surface:

The most stable configuration for nitric acid on the clean anatase (101) surface is a monodentate structure $Ti_{5c}$-ON(O)OH…$O_{2c}$(a) with a hydrogen bonded to a neighboring bridged oxygen, its adsorption energy is 13.3 kcal/mol. The $Ti_{5c}$-ON(O)OH-$O_{2c}$(a) can overcome a small barrier for H atom migration to an adjacent bridged oxygen forming $Ti_{5c}$-ON(O)O...H-$O_{2c}$(a) with an exothermicity of 0.4 kcal/mol. Similar to the reaction on the rutile (110) surface, for the rotation of ON(O)O molecule, from $Ti_{5c}$-ON(O)O...H-$O_{2c}$(a) to form $Ti_{5c}$-ON(O)O-$Ti_{5c}$,H-$O_{2c}$(a) has a barrier of 9.1 kcal/mol. The $NO_3$ elimination from $Ti_{5c}$-ON(O)O-$Ti_{5c}$,H-$O_{2c}$(a) to generate the H-$O_{2c}$(a) adsorbate and $NO_3$(g) has an endothermicity of 56.8 kcal/mol which represents the adsorption energy of $NO_3$ on H-covered anatase $TiO_2$ surface.

(4) The adsorption and reaction of the dimer nitric acid on the anatase (101) surface

Similar to the rutile surface, the 2($Ti_{5c}$-ON(O)OH....$O_{2c}$(a)) configuration is the most stable one on the anatase surface with an adsorption energy of 28.9 kcal/mol, which are slightly bigger than two times of the monodentate 13.3 kcal/mol. No intermediate structure like LM1 on rutile can be formed as shown in Figure 3-2-6. To form the configuration $Ti_{5c}$-ON(O)ON(O)O-$Ti_{5c}$,$O_{2c}$-HOH-$O_{2c}$(a) requires a higher barrier of 68.2 kcal/mol than that on the rutile surface. Formation of $Ti_{5c}$-ON(O)ON(O)O-$Ti_{5c}$,$O_{2c}$-HOH-$O_{2c}$(a) can therefore not occur spontaneously due to the high barrier. The elimination process from $Ti_{5c}$-ON(O)ON(O)O-$Ti_{5c}$,$O_{2c}$-HOH-$O_{2c}$(a) to the $Ti_{5c}$-ON(O)ON(O)O-$Ti_{5c}$(a) + $H_2O$(g) is only endothermic by 4.8 kcal/mol.

(5) Hydrogen effect

Hydrogen atom plays an important role in the adsorption energies of the adsorbates on $TiO_2$ surface. We compare the adsorption energies of reveal species with and without H atom on the bridged oxygen atom on rutile and anatase surfaces. According to our calculated results, the adsorption energies of $NO_3$(g) adsorbed on the rutile and anatase surface increase by 46.7 and 50.1 kcal/mol, respectively (see in Table 3-3(c) ), when an H atom is adsorbed on the nearest bridged oxygen atom.

By analyzing the Bader charges, the charge of ON(O)O in $Ti_{5c}$-ON(O)O-$Ti_{5c}$,H-$O_{2c}$(a) is -0.63 e and it is -0.42e in $Ti_{5c}$-ON(O)O-$Ti_{5c}$(a) on the rutile. While the charge of ON(O)O is -0.65e in $Ti_{5c}$-ON(O)O-$Ti_{5c}$,H-$O_{2c}$(a) and it is -0.43 e in $Ti_{5c}$-ON(O)O-$Ti_{5c}$(a) on the anatase. It is found that there is a charge transfer from $TiO_2$ to $NO_3$ in the presence of H atom co-adsorbed on a bridged oxygen atom, and enhances the $NO_3$ adsorption energy.

(6) $(InN)_x$, x=1, 2, 3, 6, 10 on ON(O)O-covered $TiO_2$ surface

Our calculations show that the adsorption energies of $(InN)_x$, are less than 50.2 kcal/mol on the rutile surface and 48.2 kcal/mol on the anatase surface covered with ON(O)O. By Bader charge analysis, we find that only a small electron density (0.36 e for rutile, 0.35 e for anatase) transfer from $(InN)_x$, to the ON(O)O linker. Therefore, the –ON(O)O- might not be a good linker between a semiconductor dot and the $TiO_2$ surface.

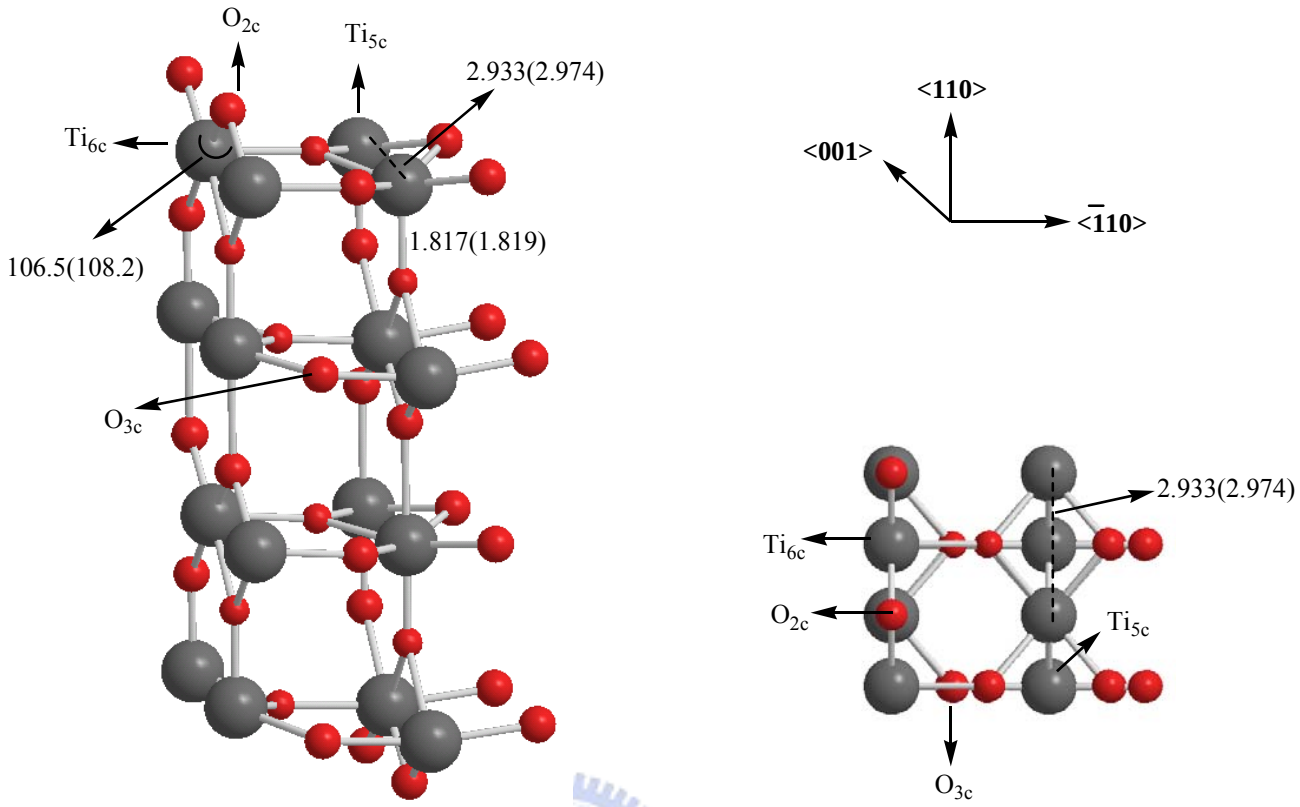


Side View Top View

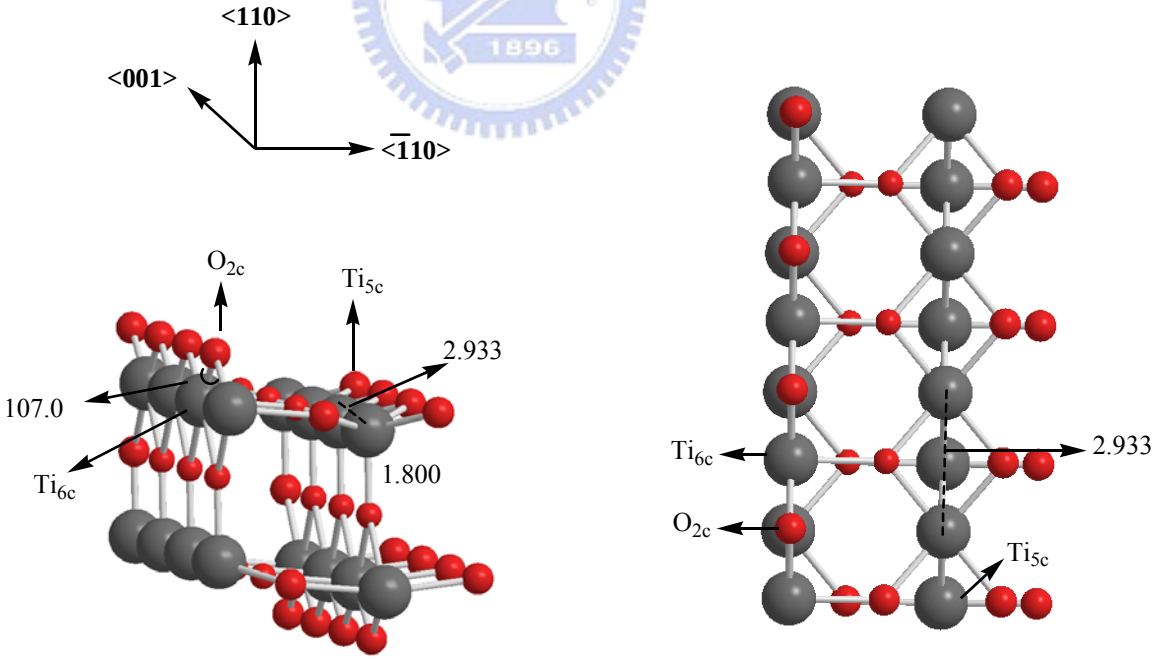


Side View Top View

**Figure 3-1-1(a) $TiO_2$ rutile (110) surface 1x2x2 super cell**
**3-1-1(b) $TiO_2$ rutile (110) surface 1x4x1 super cell**

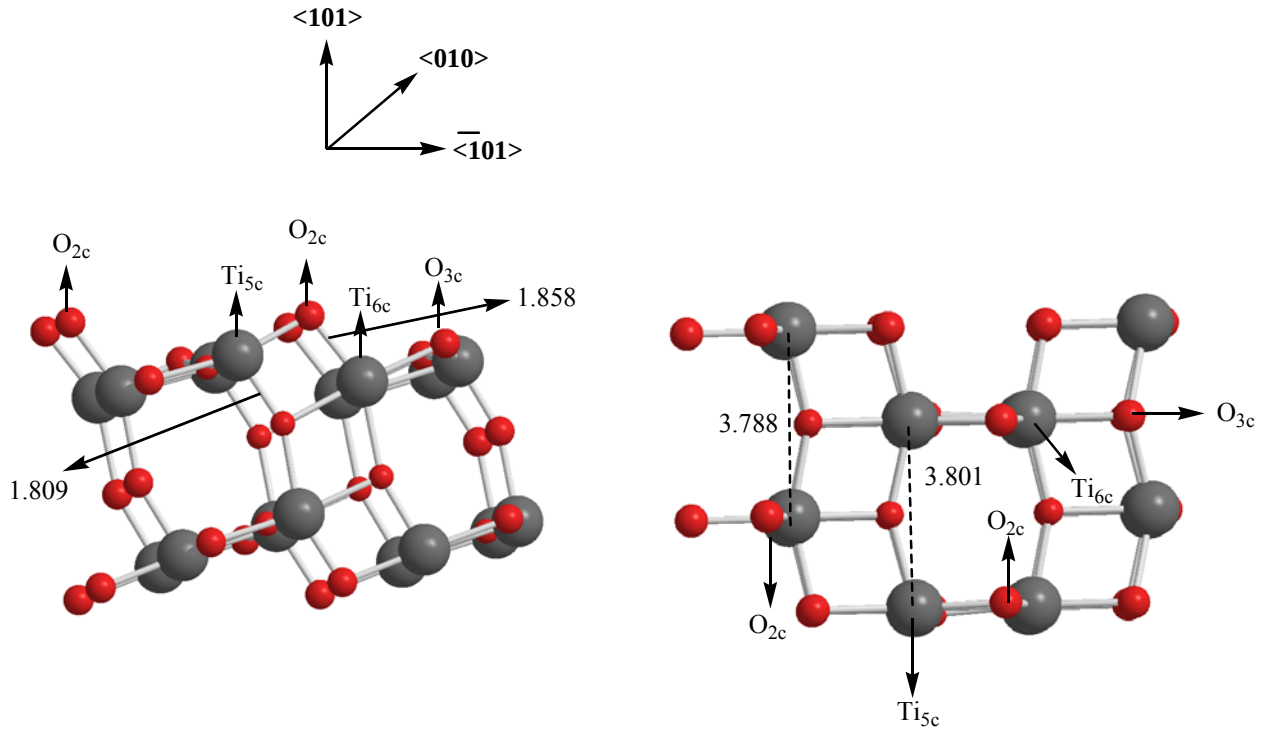


Side View Top View

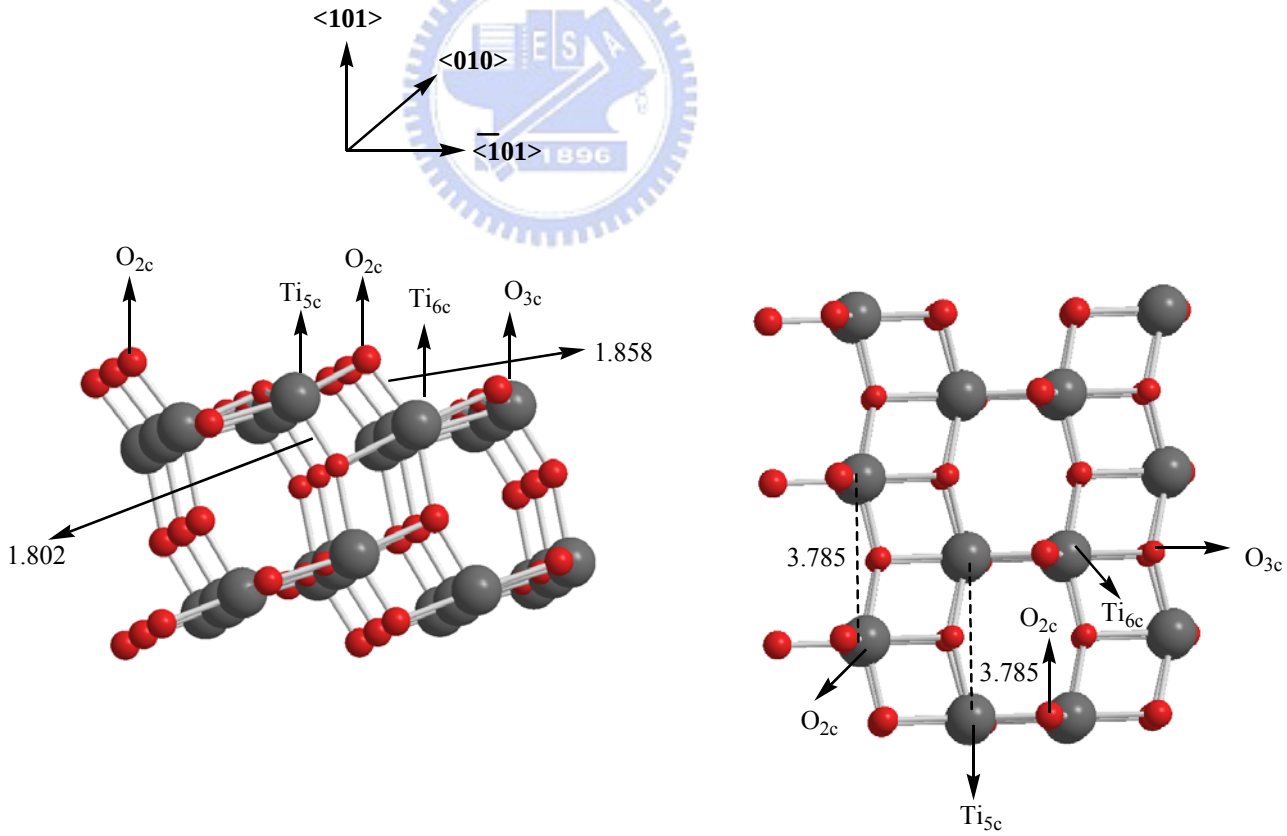


Side View Top View

**Figure 3-1-1(c) $TiO_2$ anatase (101) surface 2x1x2 super cell**

**3-1-1(d) $TiO_2$ anatase (101) surface 3x1x2 super cell**

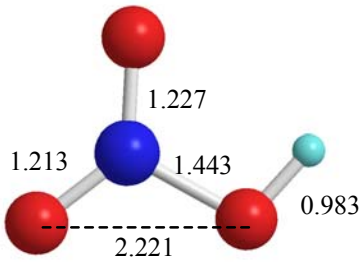


Side View

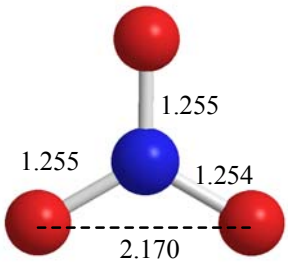


Side View

**Figure 3-1-1(e) Calculated geometry of $HNO_3$ molecule**

**3-1-1(f) Calculated geometry of $NO_3$ molecule**

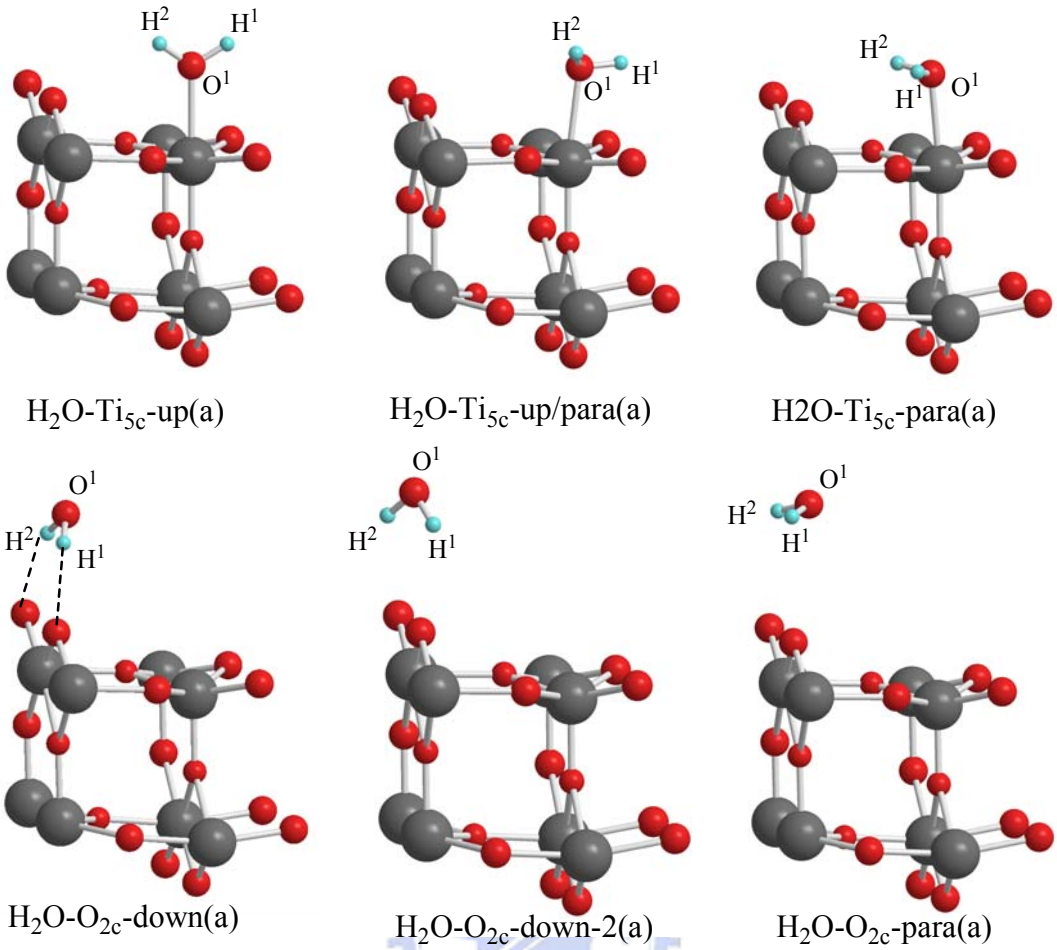


**Figure 3-1-2(a) Optimized geometries of adsorbed $H_2O$ on $TiO_2$ rutile (110) surface**

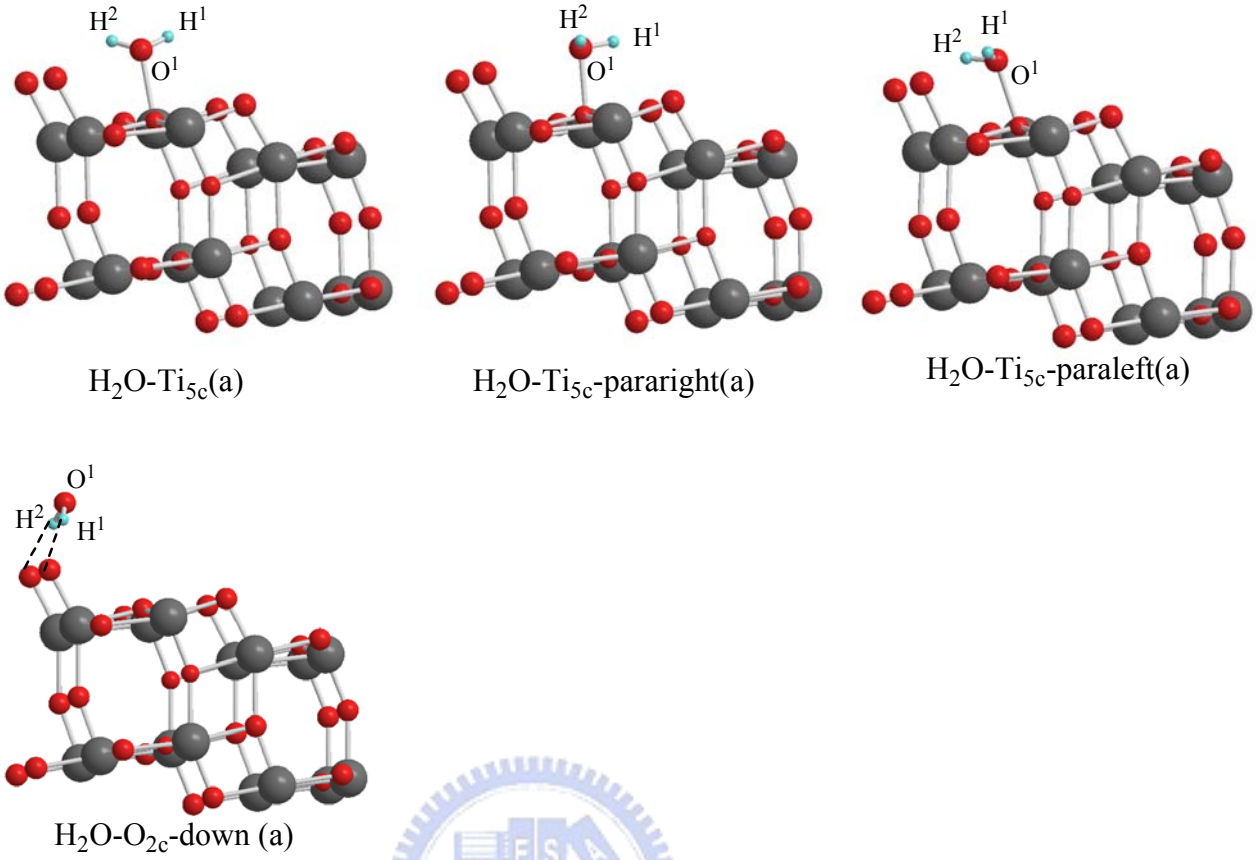


**Figure 3-1-2(b) Optimized geometries of adsorbed $H_2O$ on $TiO_2$ anatase (101) surface**

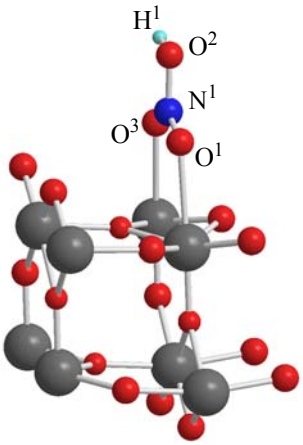


$Ti_{5c}$-ON(OH)O-$Ti_{5c}$(a)

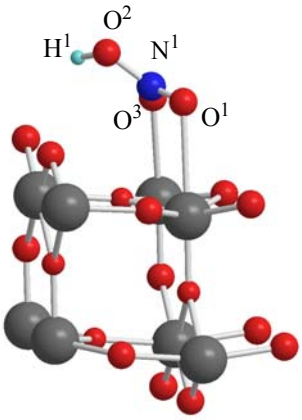


$Ti_{5c}$-ON(OH)O-$Ti_{5c}$-2(a)

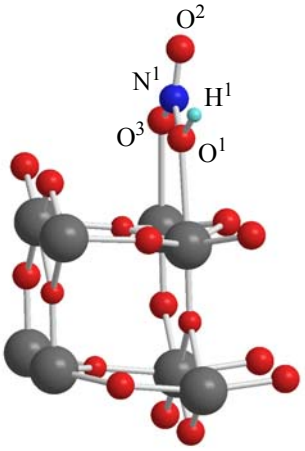


$Ti_{5c}$-O(H)N(O)O-$Ti_{5c}$(a)

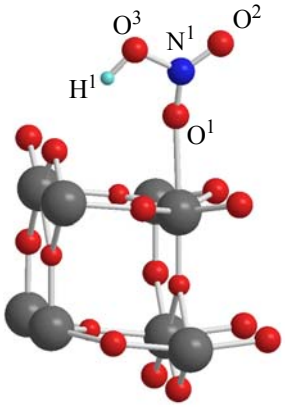


$Ti_{5c}$-ON(O)OH...$O_{2c}$(a)

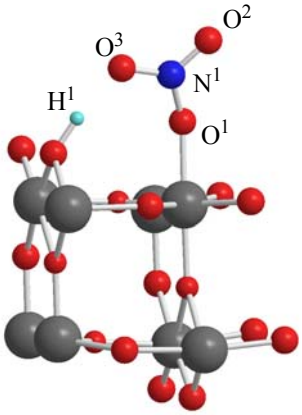


$Ti_{5c}$-ON(O)O...H-$O_{2c}$(a)

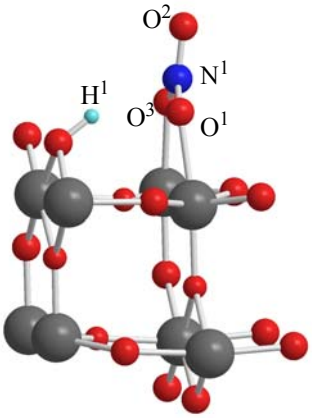


$Ti_{5c}$-ON(O)O-$Ti_{5c}$,H-$O_{2c}$(a)

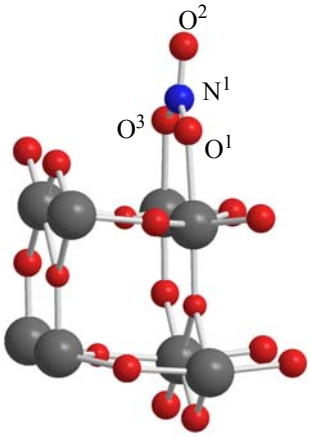


$Ti_{5c}$-ON(O)O-$Ti_{5c}$(a)

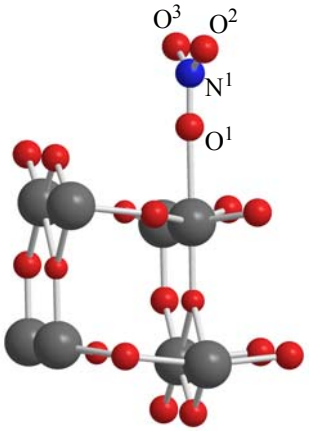


$Ti_{5c}$-ON(O)O-$Ti_{5c}$-2(a)

**Figure 3-2-1(a) Optimized geometries of adsorbed of $HNO_3$ monomer on $TiO_2$ rutile (110) surface**

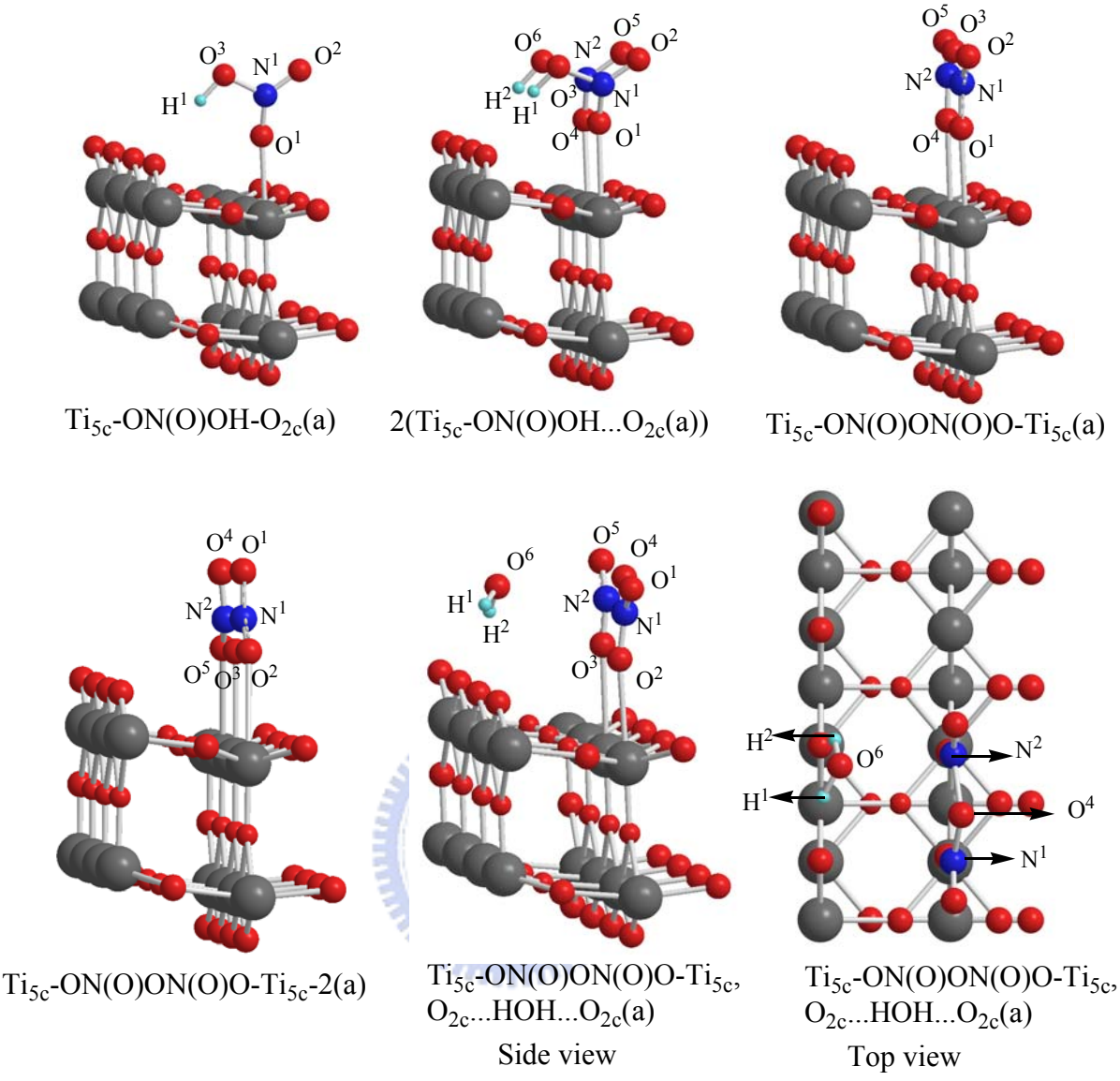


**Figure 3-2-1(b) Optimized geometries of adsorbed of $HNO_3$ dimer on $TiO_2$ rutile (110) surface**

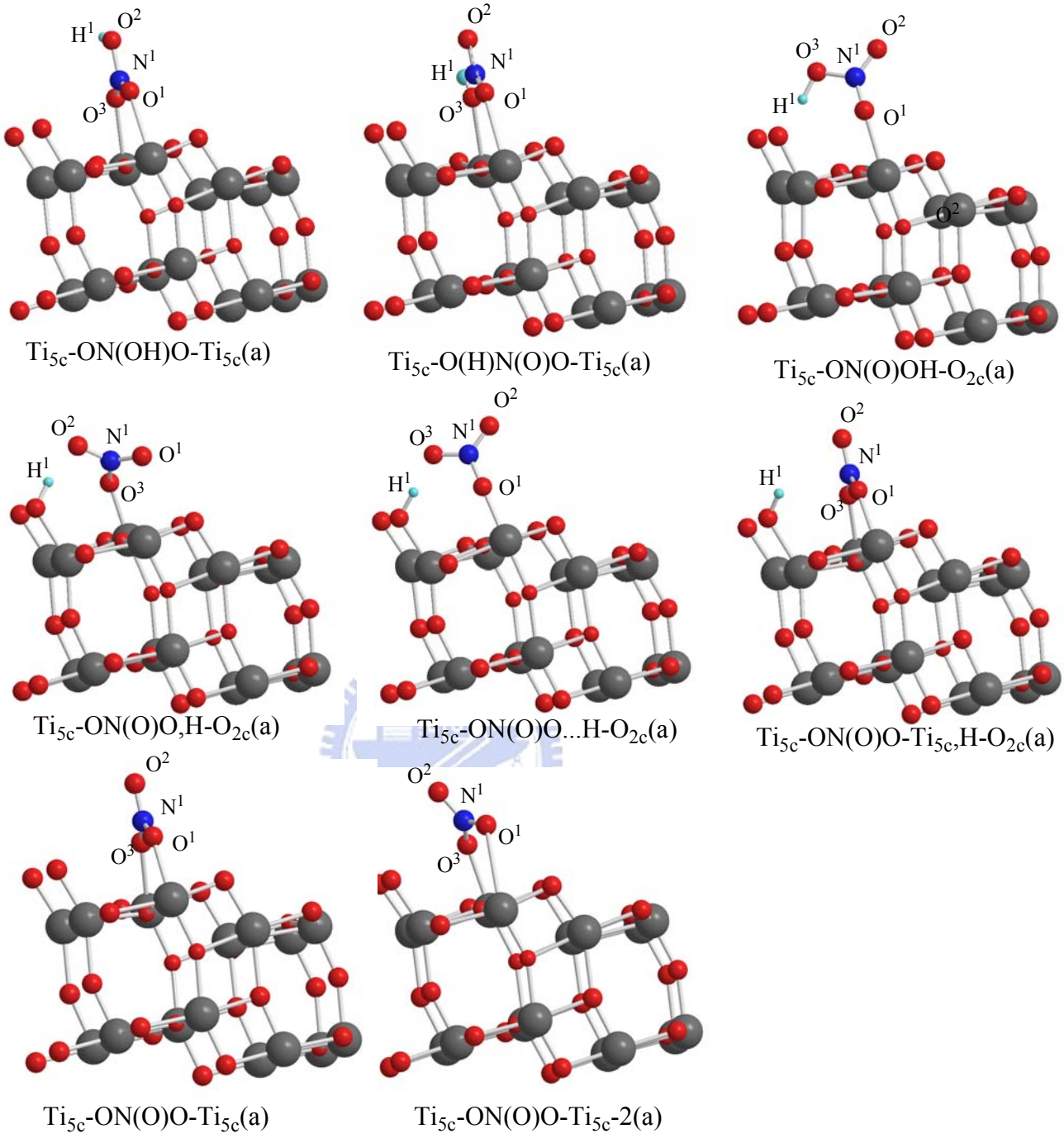


**Figure 3-2-2(a) Optimized geometries of adsorbed of $HNO_3$ monomer on $TiO_2$ anatase (101) surface**

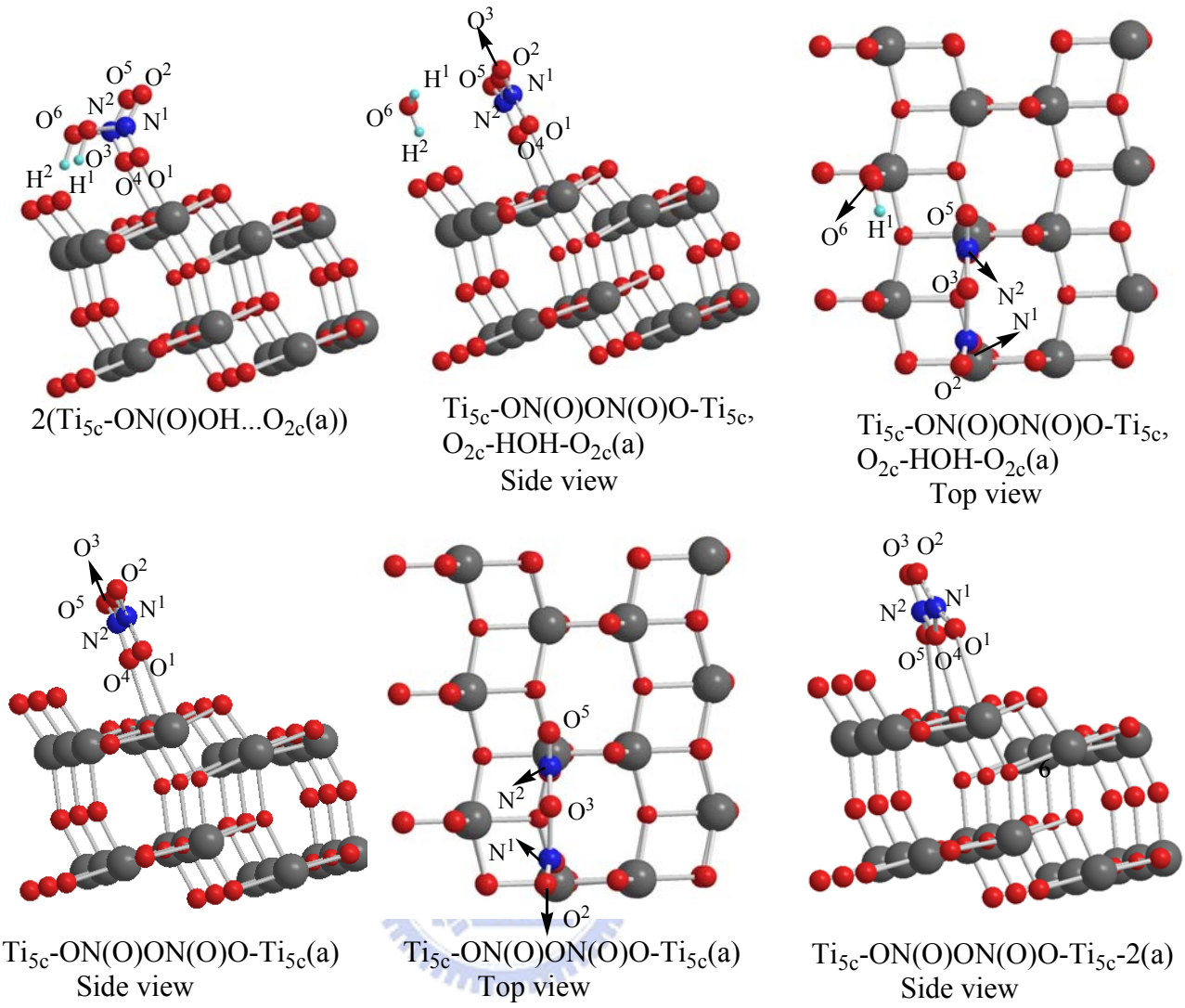


**Figure 3-2-2(b) Optimized geometries of adsorbed of $HNO_3$ dimer on $TiO_2$ anatase (101) surface**

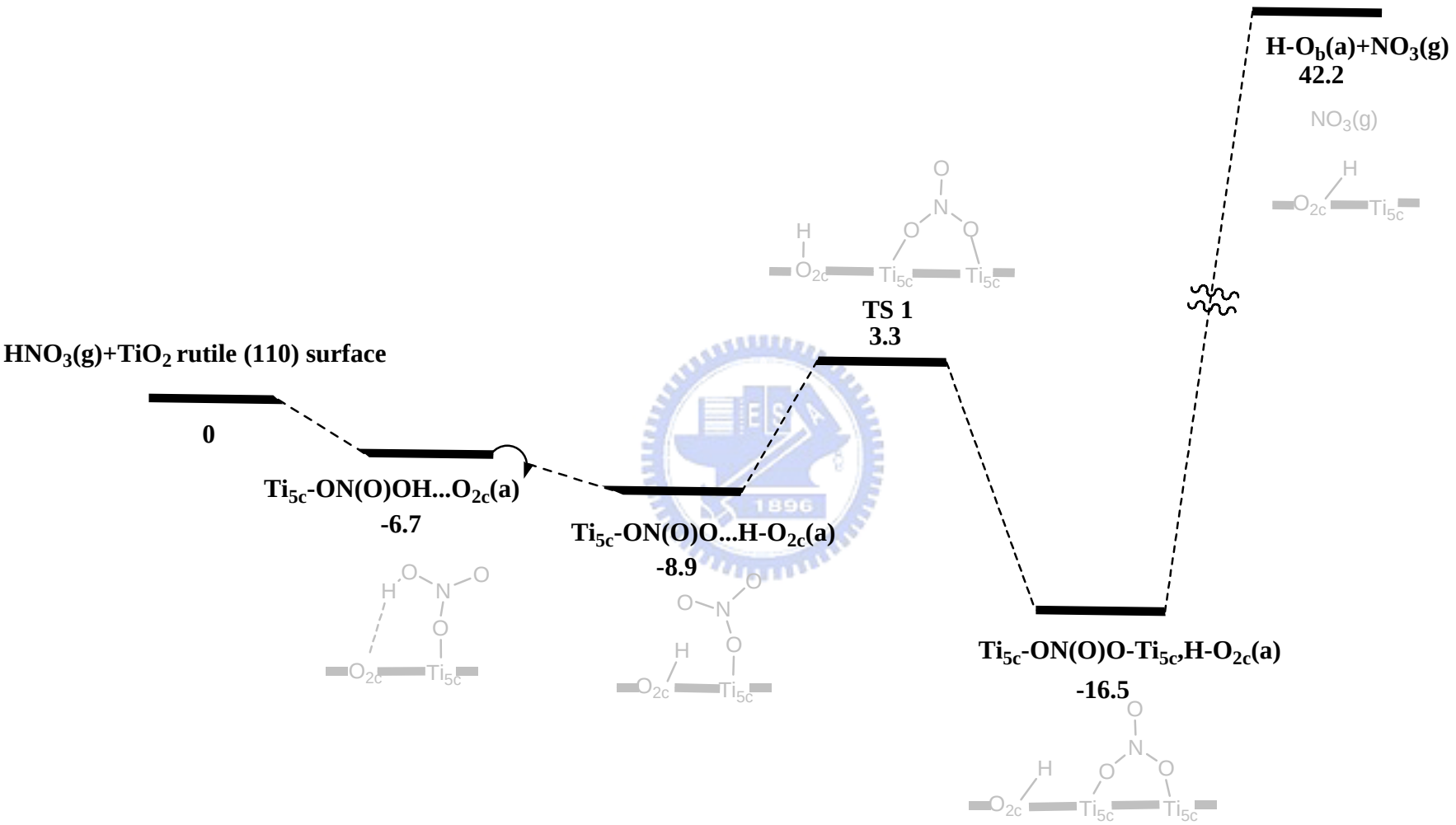


**Figure 3-2-3 Potential energy surface for the $HNO_3$ monomer on $TiO_2$ rutile (110) surface**

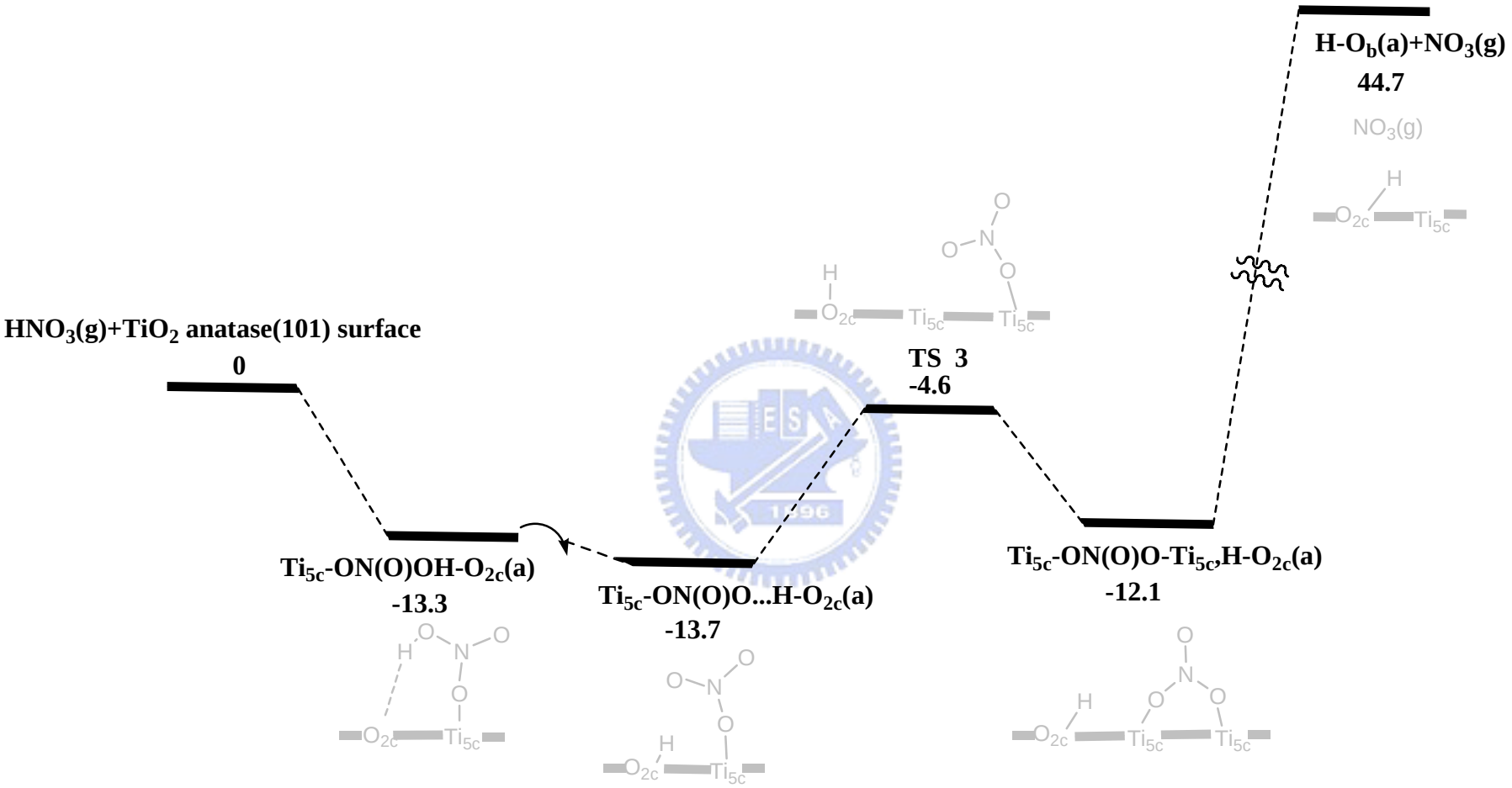


**Figure 3-2-4 Potential energy surface for the $HNO_3$ monomer on $TiO_2$ anatase (101) surface**

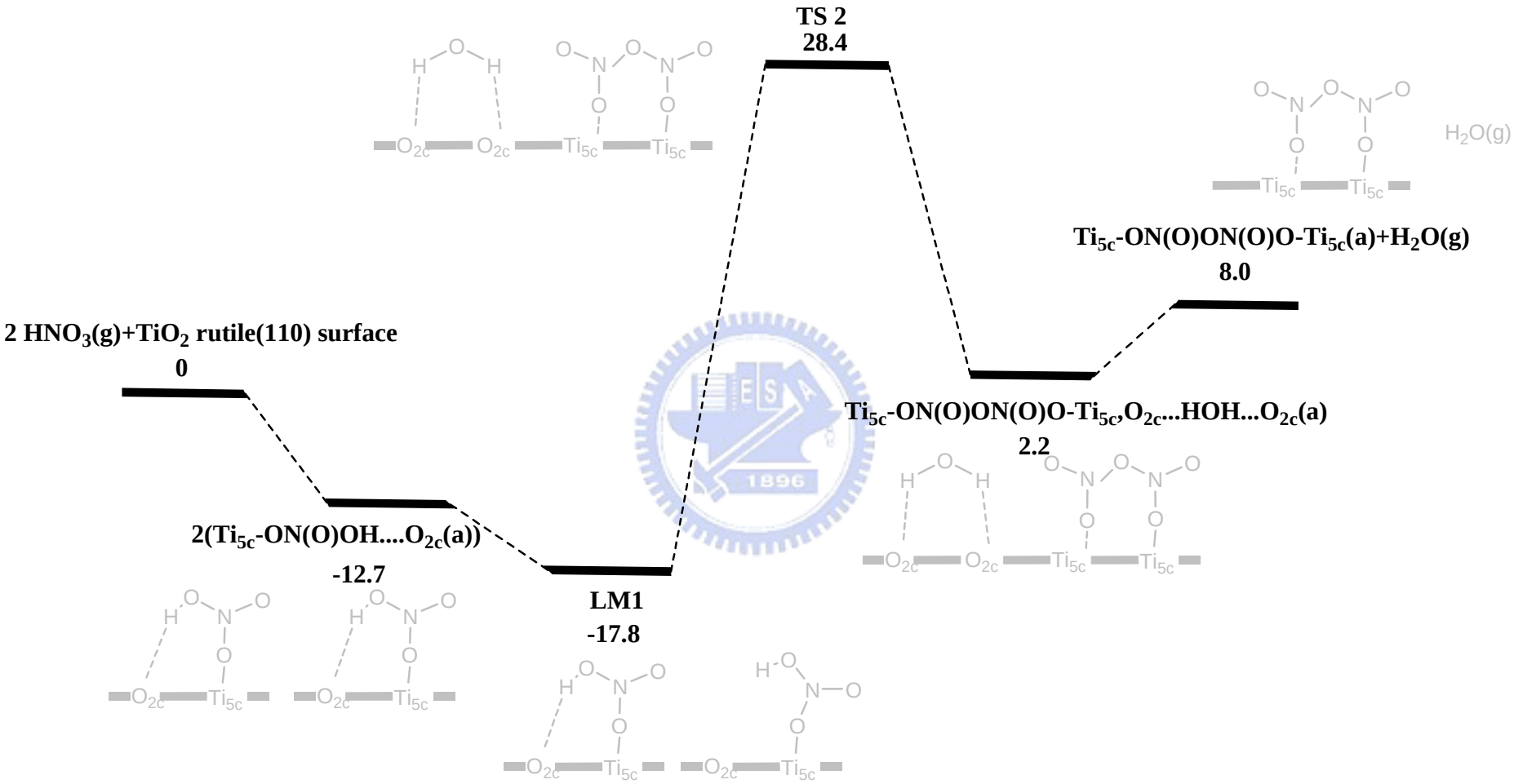


**Figure 3-2-5 Potential energy surface for the $HNO_3$ dimer on $TiO_2$ rutile (110) surface**

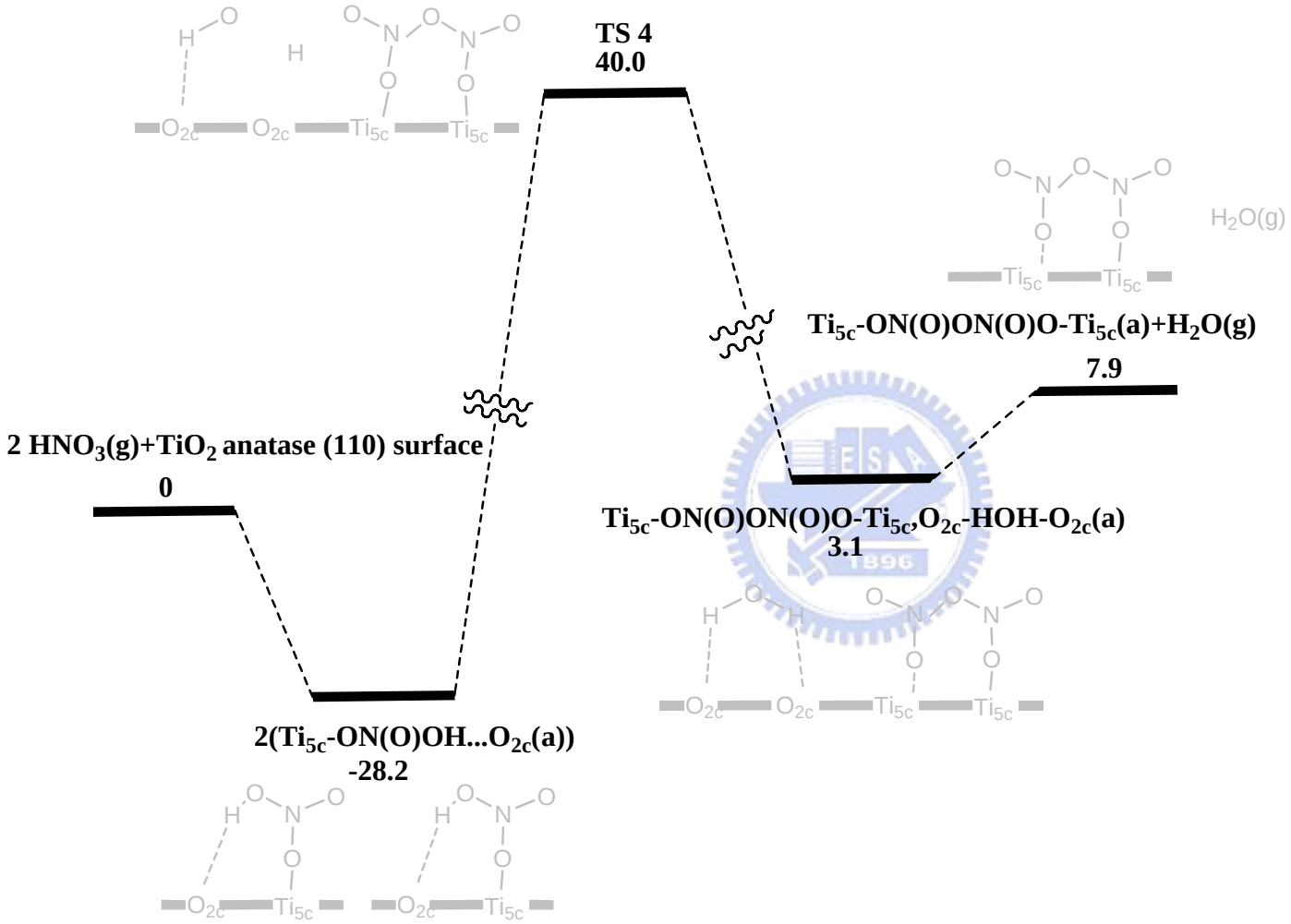


**Figure 3-2-6 Potential energy surface for the $HNO_3$ dimer on $TiO_2$ anatase (101) surface**

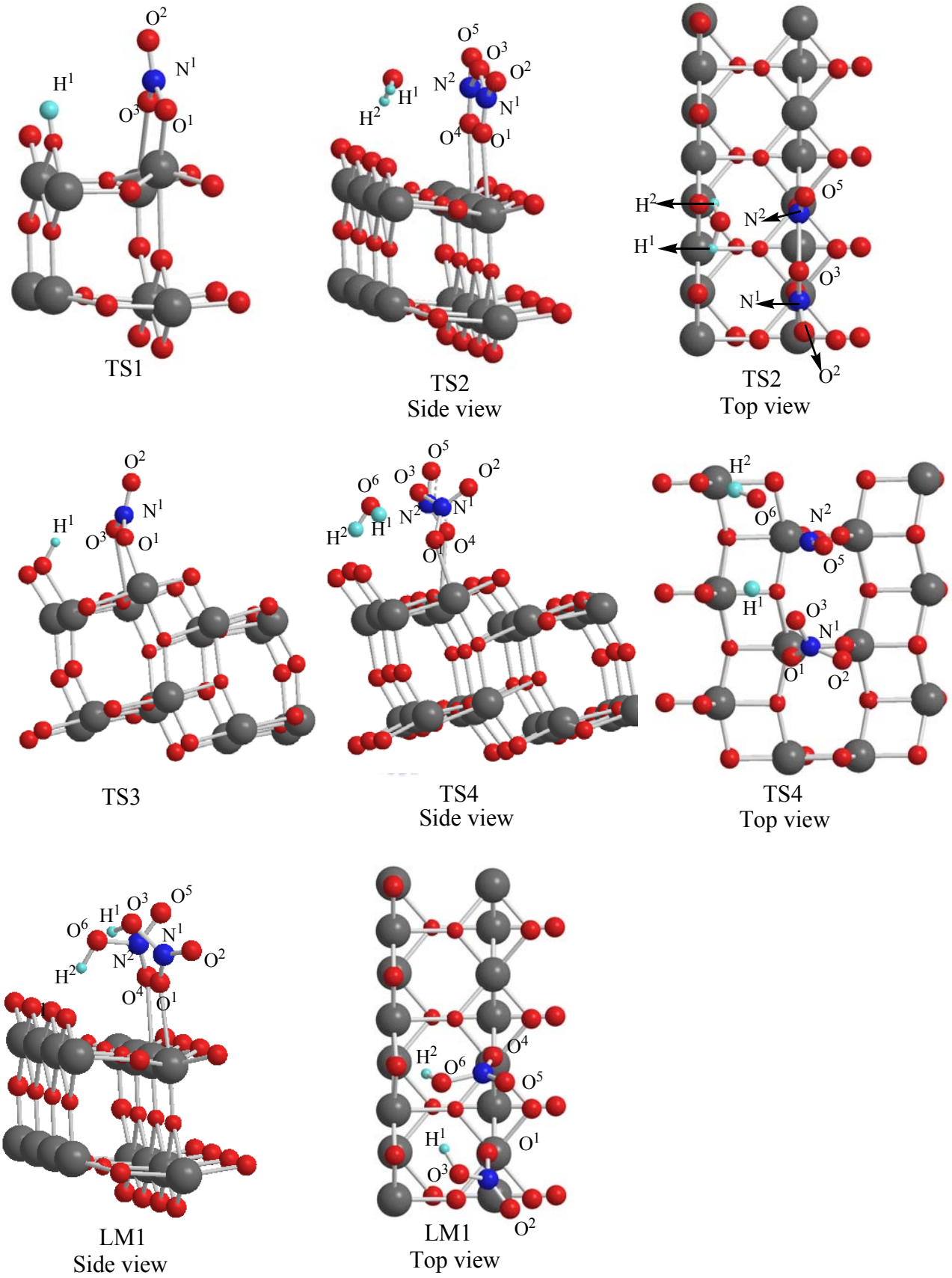


**Figure 3-2-7 Geometrical of illustrations of LM1 and TS1 TS2 TS3 TS4**

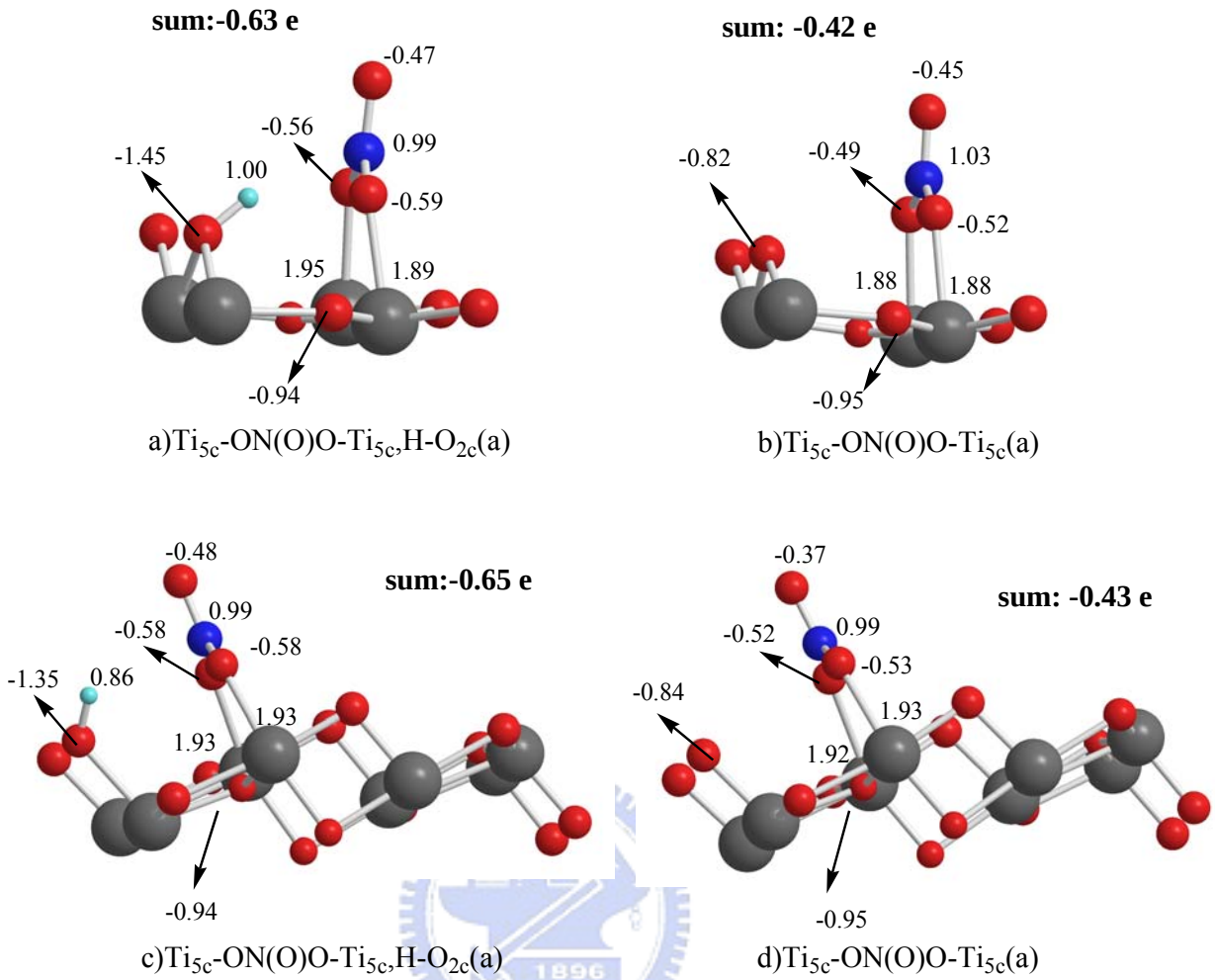


**Figure 3-4 Bader Charge Analyses**

**a),b) on rutile surface**

**c),d) on anatase surface**

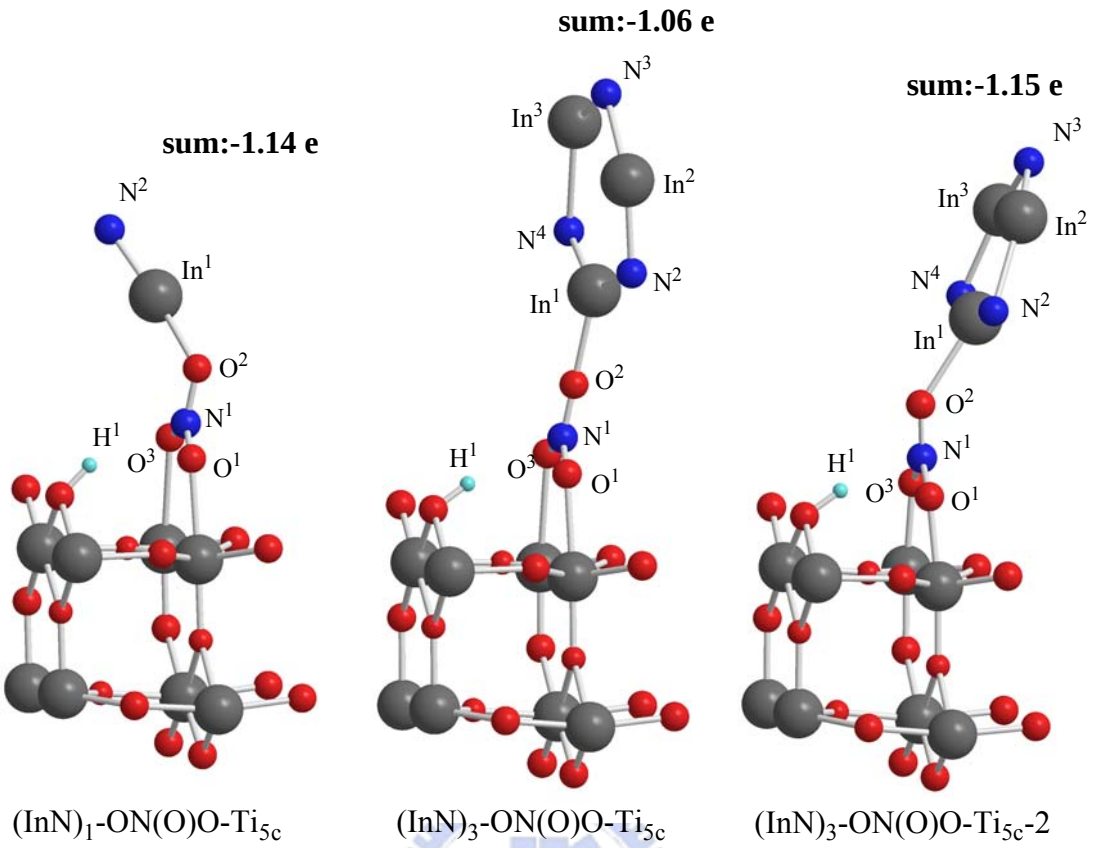


**Figure 3-5-1(a) Optimized geometries of (InN)x, x=1, 3 adsorbed on $TiO_2$ rutile (110) surface**

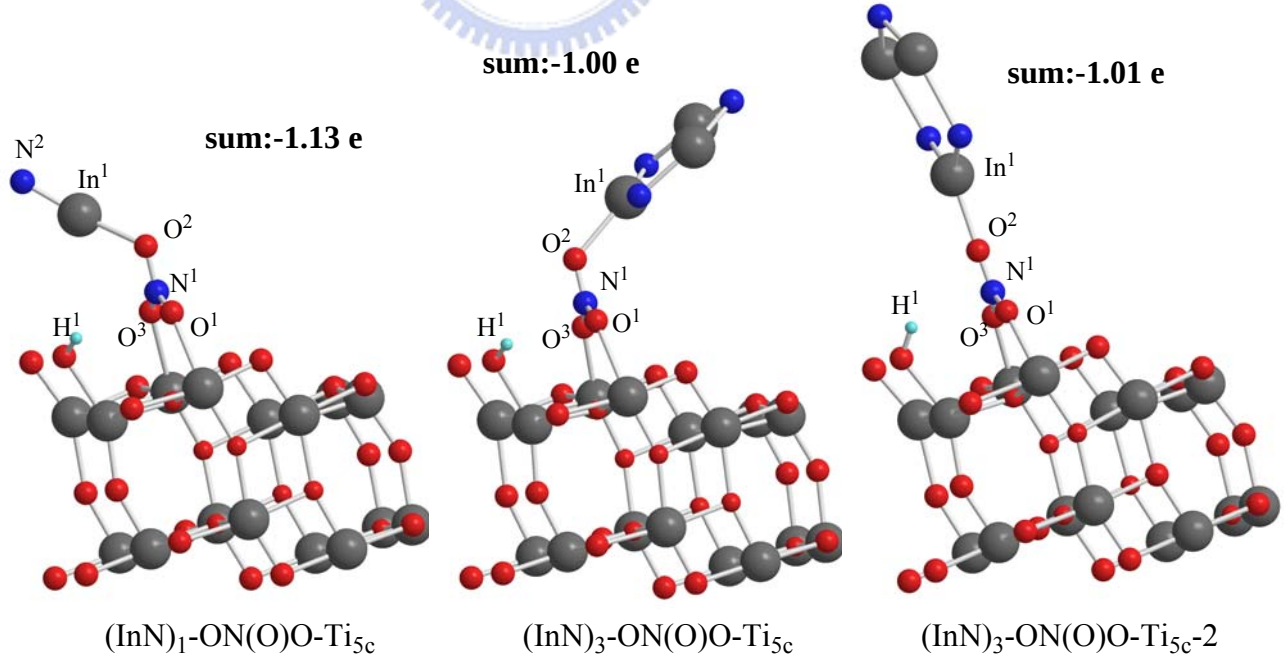


**Figure 3-5-2(a) Optimized geometries of (InN)x, x=1, 3 adsorbed on $TiO_2$ anatase (101) surface**

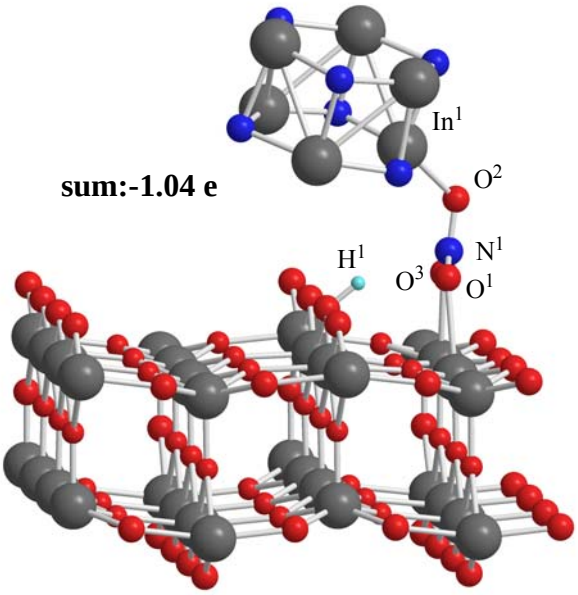


$(InN)_6$-ON(O)O-$Ti_{5c}$

Side view

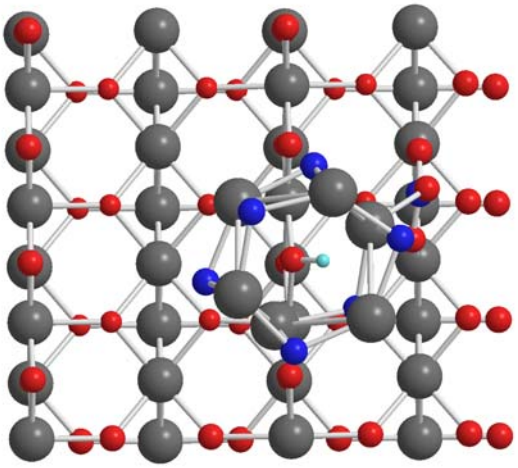

$(InN)_6$-ON(O)O-$Ti_{5c}$

Top view

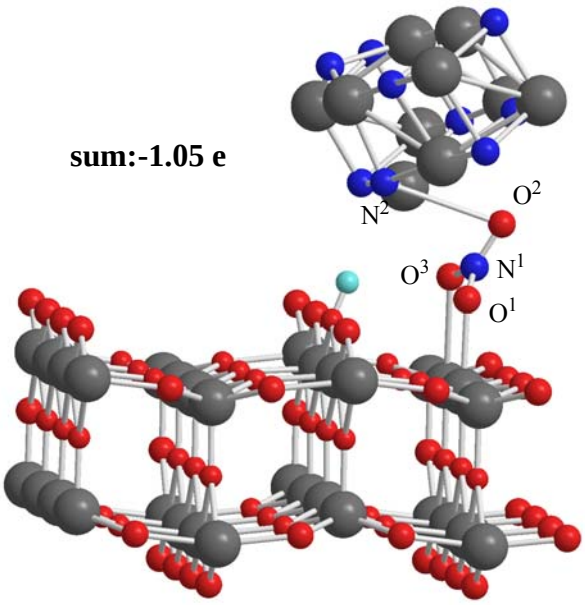


$(InN)_{10}$-ON(O)O-$Ti_{5c}$

Side view

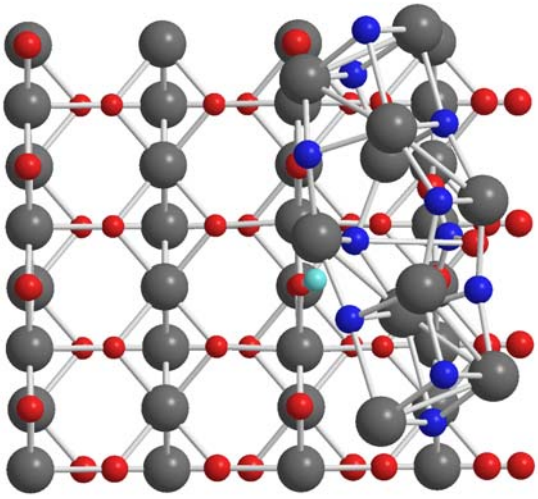

$(InN)_{10}$-ON(O)O-$Ti_{5c}$

Top view

**Figure 3-5-1(b) Optimized geometries of (InN)x, x=6, 10 adsorbed on $TiO_2$ rutile (110) surface**

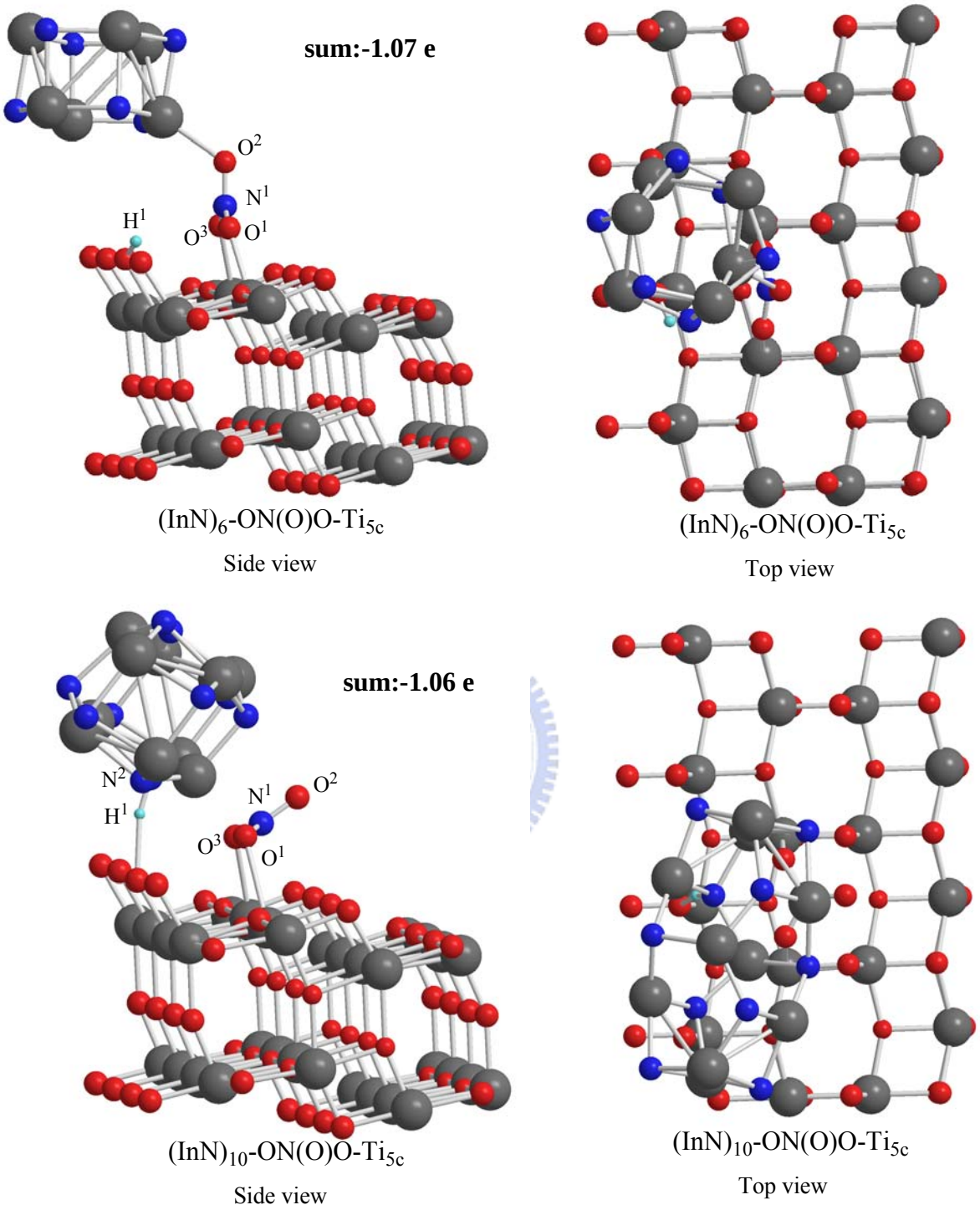


**Figure 3-5-2(b) Optimized geometries of (InN)x, x=6, 10 adsorbed on $TiO_2$ anatase (101) surface**

**Table 3-1-2(a) Optimized adsorption energies for $H_2O$ on two size of $TiO_2$ (110) surface**

| Structure | Eads rutile 1x2x2 | Eads rutile 1x4x1 |
|---|---|---|
| $H_2O$-$Ti_{5c}$-up(a) | 14.0 | 13.7 |
| $H_2O$-$Ti_{5c}$-up/para(a) | 16.6 | 14.1 |
| $H_2O$-$Ti_{5c}$-para(a) | 12.3 | 12.3 |
| $H_2O$-$O_{2c}$-down(a) | 2.3 | 3.2 |
| $H_2O$-$O_{2c}$-down-2(a) | 1.0 | -- |
| $H_2O$-$O_{2c}$-para(a) | 0.7 | -- |

**Table 3-1-2(b) Optimized bond lengths (Å) and adsorption energies for $H_2O$ on $TiO_2$ (110) rutile surface**

| Structure | $Ti_{5c}$-$O^1$ | $O^1H^1$-$O_{2c}$ | $O^1H^2$-$O_{2c}$ | $O^1H^1$-$O_{2c}^A$ | $Ti_{5c}$-$Ti_{5c}$ | $Ti_{5c}$-$O_{3c}$ | $\angle Ti_{6c}$-$O_{2c}$-$Ti_{6c}$ | Eads |
|---|---|---|---|---|---|---|---|---|
| $H_2O$-$Ti_{5c}$-up(a) | 2.240 | -- | 2.843 | -- | 2.934 | 1.869 | 104.8° | 14.0 |
| $H_2O$-$Ti_{5c}$-up/para(a) | 2.281 | -- | 3.813 | 1.887 | 2.931 | 1.884 | 104.8° | 16.6 |
| $H_2O$-$Ti_{5c}$-para(a)) | 2.270 | 2.960 | 3.509 | -- | 2.935 | 1.868 | 105.8° | 12.3 |
| $H_2O$-$O_{2c}$-down(a) | -- | 2.132 | 2.146 | -- | 2.934 | 1.817 | 106.0° | 2.3 |
| $H_2O$-$O_{2c}$-down-2(a) | -- | 2.398 | 3.090 | -- | 2.934 | 1.815 | 106.3° | 1.0 |
| $H_2O$-$O_{2c}$-para(a) | -- | 3.068 | 3.639 | -- | 2.933 | 1.818 | 106.9° | 0.7 |

$O_{2c}^A$ is the other layer next to $O_{2c}$.

**Table 3-1-2(c) Optimized bond lengths (Å) and adsorption energies for $H_2O$ on $TiO_2$ (101) anatase surface**

| Structure | $Ti_{5c}$-$O^1$ | $O^1H^1$-$O_{2c}$ | $O^1H^2$-$O_{2c}$ | $Ti_{5c}$-$Ti_{5c}$ | $Ti_{5c}$-$O_{3c}$ | $O_{2c}$-$Ti_{6c}$ | Eads | Eads (from other calc.) |
|---|---|---|---|---|---|---|---|---|
| $H_2O$-$Ti_{5c}$-up(a) | 2.262 | -- | 2.775 | 3.786 | 1.795 | 1.864 | 12.1 | |
| $H_2O$-$Ti_{5c}$-pararight(a) | 2.263 | -- | 3.153 | 3.811 | 1.791 | 1.863 | 10.5 | |
| $H_2O$-$Ti_{5c}$-paraleft(a) | 2.263 | 2.498 | 2.294 | 3.791 | 1.797 | 1.856 | 15.7 | $19.2^B$ |
| $H_2O$-$O_{2c}$-down(a) | -- | 1.949 | 2.035 | 3.783 | 1.802 | 1.857 | 1.9 | |

[B] The most stable adsorption energy of $H_2O$ on anatase surface is 19.2 kcal/mole from Raghu $H_3BO_3$ paper.

**Table 3-2-1(a) Optimized bond lengths (Å) and adsorption energies for $HNO_3$ on $TiO_2$ (110) surface**

| Structure | $Ti_{5c}$-$O^1$ | $Ti_{5c}$-$O^3$ | $O^1H^1$-$O_{2c}$ | $O^2H^1$-$O_{2c}$ | $O^3H^1$-$O_{2c}$ | $O^3$-$H^1O_{2c}$ | $Ti_{5c}$-$Ti_{5c}$ | $Ti_{5c}$-$O_{3c}$ | Eads |
|---|---|---|---|---|---|---|---|---|---|
| $Ti_{5c}$-ON(OH)O-$Ti_{5c}$(a) | 2.550 | 2.554 | -- | -- | -- | -- | 2.934 | 1.829 | 6.0 |
| $Ti_{5c}$-ON(OH)O-$Ti_{5c}$-2(a) | 2.707 | 2.547 | -- | 2.393 | -- | -- | 2.940 | 1.823 | 5.0 |
| $Ti_{5c}$-O(H)N(O)O-$Ti_{5c}$(a) | 2.520 | 2.651 | 3.740 | -- | -- | -- | 2.926 | 1.827 | 5.7 |
| $Ti_{5c}$-ON(O)OH...$O_{2c}$(a) | 2.428 | -- | -- | -- | 2.288 | -- | 2.932 | 1.838 | 6.7 |
| $Ti_{5c}$-ON(O)O...H-$O_{2c}$(a) | 2.006 | -- | -- | -- | -- | 1.632 | 2.946 | 2.002 | 8.9 |
| $Ti_{5c}$-ON(O)O-$Ti_{5c}$,H-$O_{2c}$(a) | 2.164 | 2.153 | -- | -- | -- | 3.485 | 2.921 | 1.899 | 16.5 |
| $Ti_{5c}$-ON(O)O-$Ti_{5c}$(a) | 2.194 | 2.230 | -- | -- | -- | -- | 2.922 | 1.895 | 12.0 |
| $Ti_{5c}$-ON(O)O-$Ti_{5c}$-2(a) | 2.255 | -- | -- | -- | -- | -- | 2.935 | 1.867 | 4.7 |

**Table 3-2-1(b) Optimized bond lengths (Å) and adsorption energies for $HNO_3$ dimer and its fragments on $TiO_2$ (110) surface**

| Structure | $Ti_{5c}$-$O^1$ | $Ti_{5c}$-$O^4$ | $O^6$-$H^1$ | $O^6$-$H^2$ | $O^3H^1$-$O_{2c}$ | $O^6H^2$-$O_{2c}$ | $Ti_{5c}$-$Ti_{5c}$ | $Ti_{5c}$-$O_{3c}$ | Eads |
|---|---|---|---|---|---|---|---|---|---|
| $Ti_{5c}$-ON(O)OH-$O_{2c}$(a) | 2.426 | -- | -- | -- | 2.293 | -- | 2.937 | 1.813 | 5.8 |
| 2($Ti_{5c}$-ON(O)OH....$O_{2c}$(a)) | 2.594 | 2.551 | -- | -- | 2.266 | 2.163 | 2.945 | 1.810 | 12.8[C] |
| $Ti_{5c}$-ON(O)ON(O)O-$Ti_{5c}$(a) | 2.640 | 2.723 | -- | -- | -- | -- | 2.935 | 1.802 | 2.0 |
| $Ti_{5c}$-ON(O)ON(O)O-$Ti_{5c}$-2(a) | 2.878 | 2.791 | -- | -- | -- | -- | 2.930 | 1.798 | 1.5 |
| $Ti_{5c}$-ON(O)ON(O)O-$Ti_{5c}$,$O_{2c}$...HOH...$O_{2c}$(a) | 2.689 | 2.881 | 2.909 | 2.124 | -- | -- | 2.936 | 1.810 | 7.8 |

[C] 2($Ti_{5c}$-ON(O)OH-$O_{2c}$(a))=12.31kcal/mole in1x2x2 super cell

**Table 3-2-2(a) Optimized bond lengths (Å) and adsorption energies for $HNO_3$ and its fragments on $TiO_2$ (101) surface**

| Structure | $Ti_{5c}$-$O^1$ | $Ti_{5c}$-$O^3$ | $O^2H^1$-$O_{2c}$ | $O^2$-$H^1O_{2c}$ | $O^3H^1$-$O_{2c}$ | $O^3$-$H^1O_{2c}$ | $Ti_{5c}$-$Ti_{5c}$ | $Ti_{5c}$-$O_{3c}$ | $O_{2c}$-$Ti_{6c}$ | Eads |
|---|---|---|---|---|---|---|---|---|---|---|
| $Ti_{5c}$-ON(OH)O-$Ti_{5c}$(a) | 2.575 | 2.553 | 4.943 | -- | -- | -- | 3.801 | 1.809 | 1.858 | 1.1 |
| $Ti_{5c}$-O(H)N(O)O-$Ti_{5c}$(a) | 2.706 | 2.620 | -- | -- | 3.776 | -- | 3.806 | 1.805 | 1.854 | 2.0 |
| $Ti_{5c}$-ON(O)OH-$O_{2c}$(a) | 2.302 | -- | -- | -- | 1.529 | -- | 3.808 | 1.847 | 1.845 | 13.3 |
| $Ti_{5c}$-ON(O)O,H-$O_{2c}$(a) | 3.060 | 2.187 | -- | 1.456 | -- | -- | 3.814 | 1.813 | 1.838 | 53.4[D] |
| $Ti_{5c}$-ON(O)O...H-$O_{2c}$(a) | 2.027 | -- | -- | -- | -- | 1.485 | 3.838 | 1.971 | 1.845 | 13.7 |
| $Ti_{5c}$-ON(O)O-$Ti_{5c}$,H-$O_{2c}$(a) | 2.143 | 2.159 | -- | -- | -- | 3.133 | 3.764 | 1.902 | 1.836 | 12.1 |
| $Ti_{5c}$-ON(O)O-$Ti_{5c}$-4(a) | 3.203 | 2.281 | -- | -- | -- | -- | 3.798 | 1.809 | 1.846 | 5.6 |
| $Ti_{5c}$-ON(O)O-$Ti_{5c}$(a) | 2.259 | 2.311 | -- | -- | -- | -- | 3.755 | 1.876 | 1.834 | 6.6 |

[D] dissociate

**Table 3-2-2(b) Optimized bond lengths (Å) and adsorption energies for $HNO_3$ dimer and its fragments on $TiO_2$ (101) anatase**

| Structure | $Ti_{5c}$-$O^1$ | $Ti_{5c}$-$O^4$ | $O^3$-$H^1$ | $O^6$-$H^2$ | $O^3H^1$-$O_{2c}$ | $O^6H^1$-$O_{2c}$ | $O^6H^2$-$O_{2c}$ | $Ti_{5c}$-$Ti_{5c}$ | $Ti_{5c}$-$O_{3c}$ | $O_{2c}$-$Ti_{6c}$ | Eads |
|---|---|---|---|---|---|---|---|---|---|---|---|
| 2($Ti_{5c}$-ON(O)OH....$O_{2c}$(a)) | 2.309 | 2.332 | 1.050 | 1.053 | 1.498 | -- | 1.484 | 3.807 | 1.858 | 1.849 | 28.3 |
| $Ti_{5c}$-ON(O)ON(O)O-$Ti_{5c}$, $O_{2c}$-HOH-$O_{2c}$(a) | 2.778 | 2.513 | -- | 0.960 | -- | 4.139 | 1.810 | 3.822 | 1.795 | 1.863 | -3.1 |
| $Ti_{5c}$-ON(O)ON(O)O-$Ti_{5c}$(a) | 2.778 | 2.513 | -- | -- | -- | -- | -- | 3.822 | 1.795 | 1.862 | 2.1 |
| $Ti_{5c}$-ON(O)ON(O)O-$Ti_{5c}$-2 | 3.313 | 2.857 | -- | -- | -- | -- | -- | 3.806 | 1.794 | 1.859 | 0.2 |

**Table 3-2-3 Optimized bond lengths (Å) for transition state and intermediate on $TiO_2$ surface**

| Structure | $Ti_{5c}$-$O^1$ | $Ti_{5c}$-$O^3$ | $Ti_{5c}$-$O^4$ | $O^3$-$H^1O_{2c}$ | $O_{2c}$-$H^1$ | $O^3$-$H^1$ | $N^2$-$H^1$ | $O^6$-$H^2$ | $O^3H^1$-$O_6$ | $O^6H^1$-$O_{2c}$ | $O^6H^2$-$O_{2c}$ | $Ti_{5c}$-$Ti_{5c}$ | $Ti_{5c}$-$O_{3c}$ | $O_{2c}$-$Ti_{6c}$ |
|---|---|---|---|---|---|---|---|---|---|---|---|---|---|---|
| TS1 | 2.187 | 3.361 | -- | 3.367 | 0.969 | -- | -- | -- | -- | -- | -- | 3.055 | 2.688 | 2.013 |
| TS2 | 2.676 | -- | 2.826 | -- | -- | -- | -- | 0.960 | -- | 2.826 | 1.997 | 2.938 | 1.812 | 1.839 |
| TS3 | 2.002 | 3.027 | -- | 2.526 | 0.973 | -- | -- | -- | -- | -- | -- | 3.829 | 2.001 | 1.836 |
| TS4 | 2.721 | -- | 2.221 | -- | -- | 1.873 | 2.561 | 1.011 | -- | 2.280 | 1.886 | 3.778 | 1.796 | 1.838 |
| LM1 | 2.622 | -- | 2.637 | -- | -- | -- | -- | 1.021 | 2.203 | -- | 1.669 | 2.944 | 1.816 | 1.842 |

**Table 3-3(a) Optimized bond lengths (Å) and adsorption energies for $HNO_3$ with H atoms co-adsorbed on bridged oxygen on $TiO_2$ (110) surface**

| Structure | Eads |
|---|---|
| **One hydrogen** | |
| $Ti_{5c}$-ON(OH)O-$Ti_{5c}$,H-$O_{2c}$ (a) | 4.4 |
| $Ti_{5c}$-O(H)N(O)O-$Ti_{5c}$,H-$O_{2c}$ (a) | 3.6 |
| $Ti_{5c}$-ON(O)OH...$O_{2c}$,H-$O_{2c}$ (a) | 9.9 |
| $Ti_{5c}$-ON(OH)O-$Ti_{5c}$-2,H-$O_{2c}$ (a) | 5.3 |
| **Two hydrogen** | |
| $Ti_{5c}$-ON(OH)O-$Ti_{5c}$,H-$O_{2c}$,H-$O_{2c}$ (a) | 3.4 |
| $Ti_{5c}$-O(H)N(O)O-$Ti_{5c}$,H-$O_{2c}$,H-$O_{2c}$ (a) | 2.9 |
| $Ti_{5c}$-ON(O)OH...$O_{2c}$,H-$O_{2c}$,H-$O_{2c}$ (a) | 11.7 |
| $Ti_{5c}$-ON(OH)O-$Ti_{5c}$-2,H-$O_{2c}$,H-$O_{2c}$ (a) | 10.5 |

**Table 3-3(b) Optimized bond lengths (Å) and adsorption energies for $HNO_3$ with H atoms co-adsorbed on bridged oxygen on $TiO_2$ (101) surface**

| Structure | Eads |
|---|---|
| **One hydrogen** | |
| $Ti_{5c}$-ON(OH)O-$Ti_{5c}$,H-$O_{2c}$ (a) | 2.9 |
| $Ti_{5c}$-O(H)N(O)O-$Ti_{5c}$,H-$O_{2c}$ (a) | 3.3 |
| $Ti_{5c}$-ON(O)OH-$O_{2c}$,H-$O_{2c}$ (a) | 10.5 |
| **Two hydrogen** | |
| $Ti_{5c}$-ON(OH)O-$Ti_{5c}$,H-$O_{2c}$,H-$O_{2c}$ (a) | -2.5 |
| $Ti_{5c}$-O(H)N(O)O-$Ti_{5c}$,H-$O_{2c}$,H-$O_{2c}$ (a) | 52.7 |
| $Ti_{5c}$-ON(O)OH-$O_{2c}$,H-$O_{2c}$,H-$O_{2c}$ (a) | 8.9 |

**Table 3-3(c) Adsorption Energies (kcal/mol) for some Species Calculated at the PW91 Level**

| Species | Without Hydrogen Effect | With Hydrogen Effect[E] | |
|---|---|---|---|
| Rutile/$Ti_{5c}$-ON(O)O-$Ti_{5c}$,H-$O_{2c}$ (a) | 12.0 | 58.7 | 68.9[H] |
| Anatase/$Ti_{5c}$-ON(O)ON(O)O-$Ti_{5c}$(a) | 6.6 | 56.7 | |
| $H_2S$-$Ti_{5c}$(a)[F] | 12.9 | 9.3 | |
| HS-$Ti_{5c}$(a) | 12.2 | 42.4 | |
| $H_2O$-$Ti_{5c}$(a) | 19.9 | 16.8 | |
| HO-$Ti_{5c}$(a) | 40.7 | 77.3 | |
| $Ti_{5c}$-OB(OH)O-$Ti_{5c}$(a)[G] | 53.8 | 134.6 | |

[E] The adsorption surface is considered with one hydrogen adsorbed on the $O_{2c}$ site.

$E_{ads}$= - [$E_{total/H}$ – ($E_{slab/H}$+ $E_{molecule}$)]

[F] Hunag W. F., Chen H. T. and Lin M.C.

[G] Raghunath P. and Lin M.C.

[H] The adsorption energy is considered with two hydrogen adsorbed on the $O_{2c}$ site.

**Table 3-5(a) Optimized bond lengths (Å) and adsorption energies for $(InN)_x$, x=1, 3, 6, 10 on $TiO_2$ (110) rutile surface**

| Structure | $Ti_{5c}$-$O^1$ | $Ti_{5c}$-$O^3$ | $O^2$-$In^1$ | $O^1$-$H^1O_{2C}$ | $H^1$-$O_{2C}$ | $Ti_{5c}$-$Ti_{5c}$ | $Ti_{5c}$-$O_{3c}$ | $In^1$-$N^2$ | Eads $(InN)_x$ -ON(O)O | Eads $(InN)_x$ |
|---|---|---|---|---|---|---|---|---|---|---|
| $(InN)_1$-ON(O)O-$Ti_{5c}$ | 2.306 | 2.644 | 2.180 | 2.472 | 0.975 | 2.929 | 1.857 | 1.920 | 8.3 | |
| $(InN)_3$-ON(O)O-$Ti_{5c}$ | 2.337 | 2.671 | 2.232 | 2.382 | 0.983 | 2.927 | 1.871 | 2.261 | 29.2 | |
| $(InN)_3$-ON(O)O-$Ti_{5c}$-2 | 2.063 | 2.074 | 2.347 | 2.171 | 1.013 | 2.956 | 1.842 | 2.346 | 75.4 | |
| $(InN)_6$-ON(O)O-$Ti_{5c}$ | 2.436 | 2.248 | 2.233 | 2.311 | 0.982 | 2.918 | 1.831 | 2.158 | | 14.8 |
| $(InN)_{10}$-ON(O)O-$Ti_{5c}$ | 2.225 | 2.726 | 2.895 | 2.950 | 0.985 | 2.923 | 1.861 | 2.188 | | 50.2 |

.

**Table 3-5(b) Optimized bond lengths (Å) and adsorption energies for $(InN)_x$, x=1, 3, 6, 10 on $TiO_2$ (101) anatase surface with H-adsorption**

| **Structure** | **$Ti_{5c}$-$O^1$** | **$Ti_{5c}$-$O^3$** | **$O^2$-$In^1$** | **$O^1$-$H^1O_{2C}$** | **$H^1$-$O_{2c}$** | **$Ti_{5c}$-$Ti_{5c}$** | **$Ti_{5c}$-$O_{3c}$** | **$O_{2c}$-$Ti_{6c}$** | **Eads** $(InN)_x$ -ON(O)O | **Eads** $(InN)_x$ |
|---|---|---|---|---|---|---|---|---|---|---|
| $(InN)_1$-ON(O)O-$Ti_{5c}$ | 2.346 | 2.488 | 2.185 | 2.765 | 0.979 | 3.790 | 1.847 | 1.847 | 14.5 | |
| $(InN)_3$-ON(O)O-$Ti_{5c}$ | 2.441 | 2.174 | 2.319 | 2.667 | 0.979 | 3.777 | 1.844 | 1.847 | 45.4 | |
| $(InN)_3$-ON(O)O-$Ti_{5c}$-2 | 2.143 | 2.161 | 2.233 | 2.679 | 0.976 | 3.763 | 1.901 | 1.836 | 34.6 | |
| $(InN)_6$-ON(O)O-$Ti_{5c}$ | 2.241 | 2.288 | 2.286 | 2.718 | 0.976 | 3.773 | 1.865 | 1.850 | | 10.7 |
| $(InN)_{10}$-ON(O)O-$Ti_{5c}$ | 2.677 | 2.445 | 3.645 | 3.080 | 1.828 | 3.801 | 1.821 | 1.855 | | 48.2 |

**Table 3-6(a) Bader Charge Analyses for (InN)x-ON(O)O-$TiO_2$ rutile surface**

| X | $Ti_{5c}$ / $Ti_{5c}$ | ON(O)O | (InN)x |
|---|---|---|---|
| | 2.46 / 2.46 | | |
| 0 | 2.51 / 2.50 | -0.78 | |
| 1 | 2.48 / 2.46 | -1.14 | 0.74 |
| 3 | 2.49 / 2.47 | -1.06 | 0.61 |
| 3-2 | 2.49 / 2.49 | -1.15 | 0.57 |
| 6 | 2.49 / 2.48 | -1.04 | 0.64 |
| 10 | 2.50 / 2.47 | -1.05 | 0.68 |



**Table 3-6(b) Bader Charge Analyses for (InN)x-ON(O)O-$TiO_2$ anatase surface**

| X | $Ti_{5c}$ / $Ti_{5c}$ | ON(O)O | (InN)x |
|---|---|---|---|
| | 2.46 / 2.46 | | |
| 0 | 2.53 / 2.50 | -0.78 | |
| 1 | 2.47 / 2.47 | -1.13 | 0.69 |
| 3 | 2.49 / 2.48 | -1.00 | 0.41 |
| 3-2 | 2.50 / 2.48 | -1.01 | 0.44 |
| 6 | 2.53 / 2.50 | -1.07 | 0.50 |
| 10 | 2.48 / 2.47 | -1.06 | 0.70 |